Weak form Shallow Ice Approximation models with an improved time step restriction

Igor TOMINEC[1,2], Josefin AHLKRONA[1,2,3]

[1]*Department of Mathematics, Stockholm University, SE-106 91 Stockholm, Sweden*

[2]*Bolin Centre for Climate Research, Stockholm University, SE-106 91 Stockholm, Sweden*

[3]*Swedish e-Science Research Centre, SE-100 44 Stockholm, Sweden*

Correspondence: Igor Tominec <igor.tominec@gmail.com>

ABSTRACT. The Shallow Ice Approximation (SIA) model in strong form is commonly used for inferring the flow dynamics of grounded ice sheets. The solution to the SIA model is a closed-form expression for the velocity field. When that velocity field is used to advance the ice surface in time, the time steps have to take small values due to quadratic scaling in the horizontal mesh size. In this paper, we write the SIA model in weak form and add in the Free Surface Stabilization Algorithm (FSSA) terms. We find numerically that the time step restriction scaling is improved from quadratic to linear, but only for large horizontal mesh sizes. We then modify the weak form by adding the initially neglected normal stress terms. This allows for a linear time step restriction across the whole range of horizontal mesh sizes, leading to improve efficiency. Theoretical analysis demonstrates that the inclusion of FSSA stabilization terms transitions the explicit time-stepping treatment of second derivative surface terms to an implicit approach. Moreover, a computational cost analysis, combined with numerical results on stability and accuracy, advocates for preferring the SIA models written in weak form over the standard SIA model.

INTRODUCTION

The Shallow Ice Approximation (SIA) problem is a commonly used momentum balance model which describes the non-Newtonian, viscous, gravity driven flow of the ice in grounded ice sheets (Hutter, 1983). The model is typically used either as a standalone model or in combination with the Shallow Shelf Approximation (SSA) in hybrid models for sea-level rise predictions (Goelzer and others, 2020; Seroussi and others, 2020) on time scales of a few hundred years. Another use case are paleoclimate spin-up simulations (Seroussi and others, 2019) and paleosimulations with duration 10 000 years (Weber and others, 2021) and five million years (Pollard and DeConto, 2009). The SIA model is a simplification of the nonlinear (full) Stokes problem on the premise that an ice sheet is thin, neglecting all stress-components except vertical shear stresses. The advantages of the SIA problem over the nonlinear full Stokes problem are that the standard SIA problem is linear with respect to the velocity and computationally less expensive to solve. Some of the disadvantages when compared to the nonlinear Stokes problem are: (i) the degraded model accuracy, (ii) that when coupled to the free-surface equation the simulation time steps have to be taken very small at high mesh resolutions. The time step restriction for a SIA model with an explicit or a semi-implicit discretization of the free-surface equation is of the form $\Delta t < C \Delta x^2$, where Δt is the time step, and Δx is the horizontal mesh resolution (Hindmarsh and Payne, 1996; Hindmarsh, 2001; Bueler and others, 2005; Cheng and others, 2017). Only for extremely thin ice or steep surface gradients a linear time-step restriction occurs (Cheng and others, 2017). A recent study showed that this quadratic behaviour carries over to hybrid models combining the SIA model with the SSA model (Robinson and others, 2022). Resolving complex coastal ice dynamics requires a fine spatial resolution in the horizontal direction, so that Δx may be less than 1 km locally, and a time resolution of around 0.1 years to 10 years Bueler (2023). Using the SIA velocity fields, the simulations, however, require significantly finer time resolutions due to numerical instabilities, rather than physical instabilities Bueler (2023). To alleviate the problem when considering moving ice margins, the SIA model was combined with a fully implicit time stepping scheme in (Bueler, 2016). This requires an implementation of a nonlinear iteration increasing the computational cost and is not guaranteed to converge for bedrocks with steep gradients when the horizontal resolution is fine.

The SIA model is most commonly posed in strong form from which a closed-form solution (explicit expressions) is obtained. Evaluating the closed-form solution requires (i) numerical differentiation of the ice surface position, (ii) numerical integration in the vertical direction, observed from the bedrock to the ice surface. To facilitate (ii) the mesh vertices have to be aligned over lines following the vertical direction,

i.e., extruded meshes are needed. A simpler approach to implementing the SIA model in software based on Finite Element Method (FEM) is to pose the SIA model in weak form and solve the problem as a coupled system. This is computationally more expensive as compared to evaluating a closed-form solution, but the weak form SIA models are still a linear problem with respect to the velocity, in addition allowing for fully unstructured meshes and an easier implementation using one of the FEM libraries. SIA models are implemented in a weak form in at least two of the large-scale FEM ice sheet models (Larour and others, 2012; Gagliardini and others, 2013).

FSSA (Free Surface Stabilization Algorithm) is an easy-to-implement, computationally inexpensive method for overcoming the small time steps invented for mantle convection simulations (Kaus and others, 2010), and later introduced in the scope of ice sheet modelling for the nonlinear (full) Stokes problem (Löfgren and others, 2022; Löfgren and others, 2023). One of the requirements of the stabilization method is that the governing equations are written as a system of equations in weak form.

In this paper, we consider the SIA models written as a system of equations in weak form. This makes it possible to add the FSSA stabilization terms. We discuss how the weak SIA formulation can best be implemented using FEM and how it can be combined with FSSA. We show computationally that when the SIA problem is stabilized by using the FSSA terms, the time step restriction is improved from quadratic to linear scaling in terms of the horizontal mesh size. We further modify the weak SIA formulation to the weak linear Stokes formulation, which is a full Stokes model using the SIA viscosity function. The model does not require evaluating nonlinear iterations, but at the same time includes all stress components in the momentum balance. We argue that this improves the model robustness in terms of the numerical stability, but also improves the model accuracy (as compared to the weak SIA formulation) for a negligible increase in the computational cost. For all the enhanced SIA formulations we give a theoretical performance analysis estimating the operation count, and draw a comparison towards the operation count of the standard SIA formulation. We focus our study on simplified two-dimensional ice sheet domains: slab on a slope with a surface perturbation (Cheng and others, 2017; Hindmarsh, 2001), an idealized ice cap, and a horizontal cross-section of Greenland (Morlighem and others, 2017).

The paper is organized as follows. In Section we state the different SIA and Stokes formulations that we consider in this paper, together with the free surface equation. In Section we provide information on the semi-implicit time-stepping method for solving the free-surface equation. In Section we outline the spatial discretization methods for solving the momentum balances. In Section we define the FSSA

stabilization terms and make indications on how their addition to the SIA model impacts the free surface equation. In Section we outline a computational cost analysis of the considered SIA formulations. In Section we provide the results to a set of numerical experiments assessing the time step restrictions and the error vs. runtime ratios for all the considered SIA formulations. In Section we give our final remarks.

GOVERNING EQUATIONS

In this paper, we consider ice sheets that evolve in their shape as a function of time t. A simplified two-dimensional ice sheet geometry is accounted for by a computational domain $\Omega = \Omega(t)$. One of the approaches to advance $\Omega(t)$ from time t_k to time t_{k+1} is to:

1. solve the momentum balance equations over $\Omega(t_k)$ for horizontal and vertical velocity components u_1^k and u_2^k,

2. extract the ice sheet surface velocities $u_{1,s}^k$ and $u_{2,s}^k$ from u_1^k and u_2^k respectively,

3. solve the free surface equation using $u_{1,s}^k, u_{2,s}^k$ as data coefficients to get a new ice sheet domain Ω^{k+1}.

In this section, we state the free surface equation and all the different momentum balance equations that we consider in this paper.

Free surface equation for advancing the ice surface in time

To compute the evolution of the ice surface function $h = h(x, t)$ in time we solve the free-surface equation:

$$\partial_t h = -u_{1,s}(x, h)\,\partial_x h + u_{2,s}(x, h) + a(x, h),$$

$$t > 0,\ x \in \Omega^\perp. \tag{1}$$

where $\Omega^\perp$ is a projected domain only taking into account the horizontal components of Ω. Furthermore $u_{1,s}(x, h)$ and $u_{2,s}(x, h)$ are the surface horizontal and vertical velocity functions respectively. Term $a = a(x, h)$ is the surface mass balance in this paper set to $a(x, h) = 0$. We chose to work with the free surface equation rather than the thickness equation (common when using the SIA models), as this allows for better flexibility in terms of using the free surface equation discretizations already available from the existing full Stokes model codes such as Elmer or ISSM. The two equations can be derived one from another without any spurious residual terms. Their properties in terms of the largest feasible time step do not differ from an asymptotical perspective (comparing Cheng and others (2017) and Appendix).
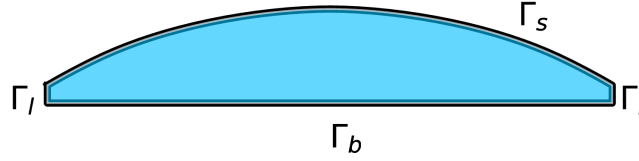
Fig. 1.   A sketch representing the ice sheet boundary $\partial\Omega$ subdivision into parts: Γ_l (the two lateral boundaries), Γ_s (the ice sheet free surface), and Γ_b (the ice sheet bedrock).

The evolution of the ice surface height h defines the evolution of shape of the domain Ω, where Ω is representing the volume of an ice sheet. The boundary of the domain $\partial\Omega \subset \mathbb{R}$ consists of three disjoint parts:

$$\partial\Omega = \Gamma_b \cup \Gamma_s \cup \Gamma_l,$$

where Γ_b is the ice sheet bedrock, Γ_s is the ice sheet free surface defined by the surface height h, and Γ_l is the ice sheet lateral boundary. A sketch of an ice sheet with the corresponding domain parts is given in Figure 1.

As is observed from (1), the surface h is a function of the velocities u_1 and u_2. The velocities are computed before solving (1), by solving the momentum balance equations (SIA or Stokes) over Ω. The coupling between h, u_1, and u_2 has an important impact on the time step restriction in the ice sheet simulations and is thus one of the main focus points of this paper.

When solving (1) we impose the boundary conditions as follows. We let the lateral margins of the ice sheet surface fixed, and use either the periodic boundary conditions:

$$h(x_L, t) = h(x_R, t), \tag{2}$$

where $x_L = \min_{x \in \Omega} x$ and $x_R = \max_{x \in \Omega} x$, or Dirichlet boundary conditions:

$$h(x_L, t) = 0, \quad h(x_R, t) = 0. \tag{3}$$

This excludes influence from nonlinearities introduced by the moving lateral boundaries, which is a complex problem in itself (Werder and others, 2013; Wirbel and Jarosch, 2020; Bueler, 2023). The margins are sometimes fixed in practice for technical reasons, see some of the models in the ISMIP6 Antartica benchmark (Seroussi and others, 2020), but it is important to get the right physical response.

Strong form nonlinear full Stokes equations

We use the full Stokes equations as a reference model for computing the velocity field $\mathbf{u} = (u_1, u_2)$ over an ice sheet geometry, when drawing the comparison towards solutions of the different SIA model formulations. This is reasonable as the SIA model is an approximation of the full Stokes equations. The full Stokes equations are:

$$-\nabla \cdot (2\mu_*(\mathbf{Du})\mathbf{Du}) + \nabla p = \rho \mathbf{g} \quad \text{on } \Omega,$$

$$\nabla \cdot \mathbf{u} = 0 \quad \text{on } \Omega, \tag{4}$$

where $\rho > 0$ is the ice density, $\mathbf{g} = (0, -9.81)\,\text{m s}^{-2}$ is the gravitational acceleration, p is the pressure, and the symmetric strain rate tensor $\mathbf{Du} = \frac{1}{2}\left(\nabla \mathbf{u} + \nabla \mathbf{u}^T\right)$ is defined through four components:

$$D_{11} = \partial_x u_1, \quad D_{12} = \frac{1}{2}(\partial_y u_1 + \partial_x u_2),$$

$$D_{21} = D_{12}, \quad D_{22} = \partial_y u_2. \tag{5}$$

The viscosity function $\mu_* = \mu_*(\mathbf{Du})$ relates the strain rates to the deviatoric stress tensor $\mathbf{Su}$ as

$$\mathbf{Su} = 2\mu_*(\mathbf{Du})\mathbf{Du}, \tag{6}$$

and is defined by:

$$\mu_*(\boldsymbol{Du}) = A(T)^{-\frac{1}{n}}\left(\frac{1}{2}\|\boldsymbol{Du}\|_F^2 + \varepsilon^2\right)^{\frac{1-n}{2n}}. \tag{7}$$

Here $n > 0$ is Glen's exponent (we use $n = 3$ throughout the paper), $A(T)$ is constant since we consider isothermal conditions and ε is the regularization parameter (a small number) which we define as in (Hirn, 2013).

In all the considered test cases we impose stress-free boundary conditions $(\mathbf{Du} - p\mathbf{I}) \cdot \mathbf{n} = 0$ at the ice sheet surface Γ_s, where $\mathbf{n}$ is the normal vector pointing outwards of Γ_s. Depending on the test case we impose either the periodic or the no-slip ($\mathbf{u} = \mathbf{0}$) boundary conditions over the ice sheet lateral boundary Γ_l. On the ice sheet bedrock Γ_b we impose no-slip boundary conditions in all test cases.

In this paper, we use full Stokes equations written in weak form (abbreviated W-Stokes) defined later in the final paragraph of Section . The full Stokes equations are nonlinear which leads to an increase in computational cost when discretized and solved on a computer, as compared to a linear problem such as the SIA equations.

Strong form SIA equations (SIA)

The SIA model is derived by using that the normal stress deviators are negligible compared to vertical shear stress. Also, due to the disparity in the order of magnitudes of the spatial derivatives of velocity components, the horizontal derivative of the vertical velocity can be neglected. The stress tensor $\mathbf{S}$ as defined in (6) is then (Greve and Blatter, 2009):

$$\mathbf{S} = \begin{bmatrix} S_{11} & S_{12} \\ S_{12} & S_{22} \end{bmatrix} \approx \begin{bmatrix} 0 & S_{12} \\ S_{12} & 0 \end{bmatrix} = \begin{bmatrix} 0 & \mu\partial_y u_1 \\ \mu\partial_y u_1 & 0 \end{bmatrix}. \tag{8}$$

The strong form SIA equations are:

$$\begin{aligned} -\partial_y \mu \partial_y u_1 + \partial_x p &= 0 \qquad \text{on } \Omega, \\ \partial_y p &= \rho g \quad \text{on } \Omega, \\ \partial_x u_1 + \partial_y u_2 &= 0 \qquad \text{on } \Omega, \end{aligned} \tag{9}$$

where $g = -9.81\,\text{ms}^{-2}$ is the second component of the gravity vector $\boldsymbol{g}$ defined in the scope of Section . The boundary conditions for (9) are:

$$\begin{aligned} u_1 &= 0 \text{ on } \Gamma_b, \quad u_2 = 0 \text{ on } \Gamma_b, \\ p &= 0 \text{ on } \Gamma_s, \ S_{12} = 0 \text{ on } \Gamma_s, \end{aligned} \tag{10}$$

where the different ice sheet domain parts are illustrated in Figure 1. We let $y \in [b(x), h(x)]$ be the vertical ice sheet coordinate, where $b(x)$ and $h(x)$ are the bedrock height and the free surface height respectively, and where x is the horizontal coordinate of an ice sheet. As the pressure is decoupled from u_1 and u_2, we first solve the second equation of (9) for pressure. We vertically integrate the equation from y to $h(x)$ and obtain:

$$p = \rho g(y - h), \tag{11}$$

where we additionally used that $p(x, y = h) = 0$. Inserting this hydrostatic pressure in the first equation of (9) and solving for $S_{12} = \mu\partial_y u_1$ using the vertical integration gives:

$$S_{12} = \rho g\, \partial_x(y - h), \tag{12}$$

where we also used that $S_{12}(x, y = h) = 0$. We then compute the SIA viscosity μ starting at the relation of fluidity Greve and Blatter (2009): $\mu^{-1} = 2A(T)\sigma_e^{n-1} = 2A(T)\|\boldsymbol{S}\|_F^{n-1}$. In the relation we first use $n = 3$ and then $\|\boldsymbol{S}\|_F^2 \approx S_{12}^2$ arising from (8). Simplifying $A(T) \approx A_0$ and taking an inverse of the fluidity relation gives $\mu = \frac{1}{2} A_0^{-1} (S_{12}^2)^{-1}$. Finally, inserting (12) gives the SIA viscosity:

$$
\begin{aligned}
\mu &= \frac{1}{2} A_0^{-1} (\rho g)^{-2} (y - h(x))^{-2} (|\partial_x h(x)|^2)^{-1} \\
&\approx \frac{1}{2} \Big(A_0(\rho g)^2 (y - h(x))^2 (|\partial_x h(x)|^2 + \varepsilon)^{-1},
\end{aligned}
\tag{13}
$$

where we have in the end also added Hirn's regularization parameter preventing the viscosity from taking infinite values where $|\partial_x h(x)|^2 \approx 0$. We observe that the SIA viscosity (13) only depends on y and $h(x)$, but not on the velocity. To derive (13) we also assumed isothermal conditions $A(T) = A_0 = 100$ MPa^{-3}yr^{-1}, where T is the temperature, but this is generally not a limitation of the SIA model. Using the viscosity function (13), the horizontal velocity u_1 is given by integrating the first equation of (9) along a vertical line from the bedrock height $b(x)$ to y, and inserting that $u_1|_{b(x)} = 0$. The vertical velocity u_2 is obtained by inserting the computed u_1 into the third equation of (9), integrating over a vertical line from $b(x)$ to y, and inserting $u_2|_{b(x)} = 0$. The closed form expressions are:

$$
\begin{aligned}
u_1 &= -\frac{1}{2} A_0 (\rho g)^3 (\partial_x h)^3 \left((y - h)^4 - (b - h)^4 \right) \\
u_2 &= \frac{1}{2} A_0 (\rho g)^3 \cdot \ldots \\
&\quad \left(\left(\frac{1}{5}(y - h)^5 - \frac{1}{5}(b - h)^5 - (b - h)^4 (y - b) \right) \cdot \ldots \right. \\
&\quad 3(\partial_x h)^2 \partial_{xx} h - (\partial_x h)^4 \left((y - h)^4 - (b - h)^4 \right) - \ldots \\
&\quad \left. 4(\partial_x b - \partial_x h)(\partial_x h)^3 (b - h)^3 \left((y - h) - (b - h) \right) \right)
\end{aligned}
\tag{14}
$$

These closed form velocity expressions are computationally inexpensive to evaluate as compared to solving the full nonlinear Stokes system. The vertical integration however requires the mesh nodes to be aligned in the vertical direction in the case of adiabatic conditions, that is, when A varies with depth.

The free surface equation requires the velocities to be evaluated at the surface. Setting $y = h$ in (14)

leads to:

$$
\begin{aligned}
u_{1,s} &= \frac{1}{2} A_0 (\rho g)^3 (\partial_x h)^3 \left((b-h)^4 \right) \\
u_{2,s} &= \frac{1}{2} A_0 (\rho g)^3 \cdot \text{...} \\
&\quad \left(\left(-\frac{3}{5}(b-h)^5 + 3(b-h)^5 \right) (\partial_x h)^2 \, \partial_{xx} h + \text{...} \right. \\
&\qquad \left. \left(4(b-h)^4 \, \partial_x b \, (\partial_x h)^2 - 3(b-h)^4 (\partial_x h)^3 \right) \partial_x h \right)
\end{aligned}
\tag{15}
$$

The derivatives in this expression are evaluated by: (i) interpolating the surface function onto a piecewise linear finite element space, (ii) taking a derivative within each element of a mesh, and (iii) L^2-projecting the element-wise derivative back to the piecewise linear finite element space.

After inserting the SIA velocities from 14 to the free surface equation 1, we write the free-surface equation problem as a nonlinear advection-diffusion PDE:

$$
\partial_t h = -u_{1,s} \, \partial_x h + u_{2,s} = C_1(h) \, \partial_x h + C_2(h) \, \partial_{xx} h,
\tag{16}
$$

where:

$$
\begin{aligned}
C_1(h) &= \frac{1}{2} A_0 (\rho g)^3 \cdot \text{...} \\
&\quad \left((b-h)^4 \, (\partial_x h)^2 + 4(b-h)^4 \, \partial_x b \, (\partial_x h)^2 - \text{...} \right. \\
&\qquad \left. 3(b-h)^4 (\partial_x h)^3 \right) \\
C_2(h) &= \frac{1}{2} A_0 (\rho g)^3 \left(-\frac{3}{5}(b-h)^5 \, (\partial_x h)^2 + 3(b-h)^5 \, (\partial_x h)^2 \right).
\end{aligned}
\tag{17}
$$

The time step restriction has a quadratic scaling in terms of the mesh size due to the second derivative term (diffusive term) $\partial_{xx} h$ in (16). The standard way to theoretically assess the timestep restriction is to linearize (16) with respect to h and then perform a von Neumann (Fourier) analysis. This was done in e.g. (Cheng and others, 2017) for the thickness equation in the case of a perturbed slab on a slope. We repeat this exercise for the free surface equation in the appendix and will revisit it for a new SIA formulation where the FSSA stabilization of (Löfgren and others, 2022; Löfgren and others, 2023) is added.

Weak form SIA equations (W-SIA)

The easiest approach to implementing the SIA equations within an existing FEM code – such as Elmer, ISSM, or FEniCS – is to write (9) in weak form and discretize the weak form using the standard finite element methods. This also allows for fully unstructured meshes, which can be of higher quality on certain

geometries, and is sometimes technically easier to construct. The weak SIA formulation is obtained by multiplying each equation of (9) using piecewise continuous test functions $v_1 = v_1(x, y), v_2 = v_2(x, y), q = q(x, y)$, respectively, and integrating over Ω. The first term of the first equation is additionally integrated by parts. In the end the weak SIA formulation is:

$$\int_\Omega \mu \partial_y u_1 \, \partial_y v_1 \, d\Omega - \int_\Omega \partial_x p \, v_1 \, d\Omega = 0,$$
$$- \int_\Omega \partial_y p \, v_2 \, d\Omega = \int_\Omega \rho g \, v_2 \, d\Omega, \tag{18}$$
$$\int_\Omega (\partial_x u_1 + \partial_y u_2) \, q \, d\Omega = 0,$$

where μ is the SIA viscosity defined in (13). In this paper we abbreviate the weak SIA formulation as W-SIA. Solving W-SIA on a computer is cheaper as compared to solving the full nonlinear Stokes system (4), since W-SIA is a linear problem due to that the viscosity is not a function of the computed velocity. W-SIA is possible to solve in terms of three subsequent matrix systems: first for pressure, secondly for u_1, and lastly for u_2. This only holds as long as W-SIA is not further stabilized using the additional stabilization terms that couple the velocity functions. A disadvantage when solving W-SIA is that the many stress components are not present in (18). This implies that the full stress term $\mathbf{Su}$ is not guaranteed to have an upper bound when the problem is solved on a computer and the mesh size approaches zero. A consequence is potentially sharp velocity gradients that deteriorate the numerical stability as well as the solution accuracy.

Under the assumption that the PDE data is regular enough, the solution to the weak formulation is identical to that of the strong formulation. However, we do not expect this to be true numerically across W-SIA (18) and SIA (9), as the surface derivatives in the closed form SIA solution (15) are evaluated numerically. The differences across the solutions are highly dependent on the choice of the numerical evaluation of the derivatives. This is also a potential source of the differences across the two formulations in the largest feasible time step when using the velocities to advance the surface function in time.

Weak form linear Stokes equations employing the SIA viscosity function (W-SIAStokes)

We add the missing stress components back to (18) resulting in the following weak formulation:

$$\int_\Omega 2\mu \partial_x u_1 \, \partial_x v_1 \, d\Omega + \int_\Omega \mu(\partial_y u_1 + \partial_x u_2) \, \partial_y v_1 \, d\Omega + ...$$

$$... - \int_\Omega \partial_x p \, v_1 \, d\Omega = 0,$$

$$\int_\Omega \mu(\partial_y u_1 + \partial_x u_2) \, \partial_x v_2 \, d\Omega + \int_\Omega 2\mu \partial_y u_2 \, \partial_y v_2 \, d\Omega + ... \tag{19}$$

$$... - \int_\Omega \partial_y p \, v_2 \, d\Omega = \int_\Omega \rho g \, v_2 \, d\Omega,$$

$$\int_\Omega (\partial_x u_1 + \partial_y u_2) \, q \, d\Omega = 0.$$

We abbreviate 19 as W-SIAStokes, as that formulation combines the full Stokes problem and the SIA viscosity function. W-SIAStokes is a linear problem, computationally less expensive to solve as compared to the full nonlinear Stokes problem. However, the system can no longer be solved as three separate matrix systems as is the case in the unstabilized W-SIA formulation (18). An advantage of W-SIAStokes over W-SIA is a guaranteed bound over the full stress term **Su**, which improves the numerical stability properties as the mesh size goes to 0.

We note that the nonlinear full Stokes problem (4) but written in weak form (W-Stokes) takes exactly the same form as W-SIAStokes (19), where we use the (full) viscosity function (7) instead of the SIA viscosity (13).

FINITE DIFFERENCE DISCRETIZATION OF THE FREE SURFACE EQUATION

We first denote that $h = h(x, t)$, and discretize the free surface equation (1) in time using the first order semi-implicit Euler method. This results in:

$$\frac{h^{k+1} - h^k}{\Delta t} = -u_{1,s}^k \partial_x h^{k+1} + u_{2,s}^k, \qquad k = 1, 2, 3, .. \tag{20}$$

where h^k, h^{k+1} are $h(x, t_k)$, $h(x, t_{k+1})$ respectively, and where $u_{1,s}^k$, $u_{2,s}^k$ are the surface velocities $u_1(x^k, y_s^k)$, $u_2(x^k, y_s^k)$ extracted from the bulk velocity functions defined over an ice sheet domain Ω^k at t_k. We note that $x \in \Omega^\perp$, where this domain is defined in the scope of Section . Now we discretize the spatial derivatives in (20) using the second-order accurate centered finite difference stencil weights, resulting in the following

system of equations:

$$\frac{\boldsymbol{h}^{k+1} - \boldsymbol{h}^k}{\Delta t} = -\mathrm{diag}(\boldsymbol{u}_{1,s}^k)\boldsymbol{D}_x\boldsymbol{h}^{k+1} + \boldsymbol{u}_{2,s}^k, \qquad k = 1, 2, 3, .. \tag{21}$$

where $h_i^{k+1} = h(x_i, t_{k+1})$, $h_i^k = h(x_i, t_k)$, $(u_1^{k+1})_i = u_1(x_i, y_s)$, $(u_2^{k+1})_i = u_2(x_i, y_s)$, $i = 1, .., N$. The components of the matrix $\boldsymbol{D}_x$ are defined by the second-order accurate finite difference stencil weights that discretize the first-order derivative operator. The final time-stepping iteration scheme is:

$$\boldsymbol{h}^{k+1} = (\boldsymbol{I} + \Delta t \, \mathrm{diag}(\boldsymbol{u}_{1,s}^k)\boldsymbol{D}_x)^{-1}(\boldsymbol{h}^k + \Delta t \, \boldsymbol{u}_{2,s}^k), \qquad k = 1, 2, 3, .. \tag{22}$$

We impose the boundary conditions as described within the scope of Section by reducing the system of equations (22) in the unknowns related to the Dirichlet conditions, or by transforming the $\boldsymbol{D}_x$ matrix into a circulant matrix in the case when we use the periodic boundary conditions.

Using a fully implicit scheme would require access to u_1^{k+1}, u_2^{k+1}, but this is computationally expensive as the velocity functions and the surface position are coupled. The surface h depends on u_1^{k+1}, u_2^{k+1} due to (20), while the velocities depend on the surface that determines the shape of the computational domain Ω on which we solve the momentum balance equations. As a consequence, computing u_1^{k+1}, u_2^{k+1} requires an expensive nonlinear iteration as demonstrated in the SIA model case in (Bueler, 2016).

FINITE ELEMENT DISCRETIZATION OF THE SIA / STOKES MODELS

Throughout the paper, we use FEM not only to solve partial differential equations in weak form, but also to evaluate the surface gradient functions. The meshes we use are extruded. To create a two-dimensional ice sheet mesh we first generate a rectangular mesh with dimensions $[x_{\min}, x_{\max}] \times [0, 1]$, where $x_{\min}$ and $x_{\max}$ are the minimum and maximum horizontal coordinates of the ice sheet geometry. Then we transform the vertical mesh coordinates using an ice sheet initial surface function.

When evaluating the SIA velocities using the closed-form expression (14) we employ FEM to evaluate $\partial_x h$, the gradient of the ice sheet surface. We first interpolate h into a piecewise linear finite element space. After that we compute the gradient $\partial_x h|_{K_i}$, $i = 1, .., N$ over each mesh element K_i. As the gradient of the piecewise linear function across the element interfaces is discontinuous (not well defined), we L_2 project the computed gradients back into a piecewise linear finite element space. By that, we compute a continuous (well-defined) surface gradient.

When solving the nonlinear Stokes problem (4) in the weak form we use Taylor-Hood elements (P2P1) to fulfill the inf-sup condition (Babuška, 1973; Brezzi, 1974), that is, piecewise quadratic polynomials for approximating the velocity functions, and piecewise linear polynomials for approximating the pressure function. This is a requirement to make the finite element discretization numerically stable.

When solving W-SIAStokes (19) we use the same type of elements as in the nonlinear Stokes problem case, for the very same reasons related to numerical stability.

When solving W-SIA the inf-sup condition does not need to be fulfilled, and we can therefore use piecewise linear finite elements (P1P1) for approximating the velocity functions as well as the pressure function. This is an advantage as the amount of unknowns when using P1P1 elements is smaller as compared to when using P2P1 elements. This is attributed to the fact that P2 finite element spaces require an addition of three midpoints over the edges of a triangle in a mesh, which then increases the total count of the degrees of freedom.

FREE SURFACE STABILIZATION ALGORITHM (FSSA) FOR THE SIA / STOKES MODELS

In (Löfgren and others, 2022; Löfgren and others, 2023) the authors introduced FSSA for the full nonlinear Stokes model to mimic an associated implicit solver advancing the ice surface from time t_k to time t_{k+1}, $k = 1, .., N$, where $t_{k+1} > t_k$. This is done by predicting the gravitational force in the weak form at t_{k+1} by adding an extra surface force term:

$$\int_{\Omega^{k+1}} \rho g \, v_2 \approx \int_{\Omega^k} \rho g \, v_2 + \theta \Delta t \int_{\partial \Omega^k} \left(\mathbf{u} \cdot \mathbf{n} \right) \rho g \, v_2 \, ds. \tag{23}$$

Here $\theta \in [0, 1]$ is a user-defined constant parameter. The relation (23) was derived from a finite difference discretization of the Reynolds transport theorem (the multi-dimensional Leibniz rule). The FSSA thus relies on the assumption that the flow is predominantly gravity-driven so that computing the gravitational force at t_{k+1} leads to a good approximation of the ice flow at t_{k+1}. This in turn enables taking larger time steps when solving the free-surface equation. Hence an implicit discretization (Löfgren and others, 2022; Löfgren and others, 2023). From a physics standpoint, the FSSA term is an extra surface pressure term acting as a damping term – when the ice is rising, the FSSA term acts as an extra surface pressure, and when the ice is sinking, it reduces the pressure. FSSA was originally introduced by (Kaus and others,

2010) for mantle convection simulations.

In this paper, we add the FSSA stabilization term to the vertical momentum balance equation. In the W-SIAStokes case (19) (and similar in the W-Stokes case) the vertical momentum balance equation becomes:

$$\int_\Omega \mu(\partial_y u_1 + \partial_x u_2)\,\partial_x v_2\,d\Omega + \int_\Omega 2\mu\partial_y u_2\,\partial_y v_2\,d\Omega + ...$$
$$... - \int_\Omega \partial_y p\,v_2\,d\Omega = \int_\Omega \rho g\,v_2\,d\Omega + \theta\Delta t \int_{\partial\Omega} (\mathbf{u}\cdot\mathbf{n})\,\rho g\,v_2\,ds. \tag{24}$$

In the W-SIA case (18) the vertical momentum balance, after adding the FSSA stabilization term, becomes:

$$- \int_\Omega \partial_y p\,v_2\,d\Omega = \int_\Omega \rho g\,v_2\,d\Omega + \theta\Delta t \int_{\partial\Omega} (\mathbf{u}\cdot\mathbf{n})\,\rho g\,v_2\,ds. \tag{25}$$

In this case, it is the added FSSA term that couples the pressure to surface velocities $\mathbf{u}_s$. Without the FSSA term the pressure is decoupled from the velocity, reducing the computational cost of the solution procedure. The coupling is however essential for numerical stability reasons.

Effects of the added FSSA terms on W-SIA

The FSSA term is using the discretized free-surface equation (22) to estimate how the force of gravity will change between times t_k and t_{k+1}. The argumentation is provided as follows. Assume the domain Ω is such that the horizontal and vertical integration can be separated, i.e., $\int_\Omega (\cdot)d\Omega = \int_{\Omega^\perp} \int_y (\cdot)dy\,dx$, where $\Omega^\perp$ only contains the horizontal coordinates of Ω and is defined in the scope of (1). Then the vertical momentum equation (25), after setting $\theta = 1$, becomes:

$$- \int_{\Omega^\perp} \int_b^{h^k} \partial_y p\,v_2\,dy\,dx = \int_{\Omega^\perp} \int_b^{h^k} \rho g\,v_2\,dy\,dx + ...$$
$$... + \Delta t \int_{\Gamma_s^k} (\mathbf{u}\cdot\mathbf{n})\,\rho g\,v_2\,ds. \tag{26}$$

As the normal vector and the arc length of a surface are respectively defined as $\boldsymbol{n} = (-\partial_x h, 1)/\sqrt{(\partial_x h)^2 + 1^2}$ and $ds = \sqrt{(\partial_x h)^2 + 1^2}\,dx$, we have that $(\boldsymbol{u}\cdot\boldsymbol{n})\,ds = (-u_{1,s}\partial_x h + u_{2,s})\,dx$. Using that, and (20) to make an

additional relation to the discretized free-surface equation, we write the FSSA term in (26) as:

$$\Delta t \int_{\Gamma_s^k} (\mathbf{u} \cdot \mathbf{n}) \, \rho g \, v_2 \, ds = \Delta t \int_{\Omega^\perp} \rho g \left(-u_{1,s} \partial_x h + u_{2,s} \right) v_2 \, dx$$
$$= \int_{\Omega^\perp} \rho g \left(h^{k+1} - h^k \right) v_2 \, dx \tag{27}$$

We now look at the expression $\left(h^{k+1} - h^k \right) v_2$ as a left point rule approximation of the integral $\int_{h^k}^{h^{k+1}} v_2 \, dy$. Then we have $\int_{\Omega^\perp} \rho g \left(h^{k+1} - h^k \right) v_2 \, dx \approx \int_{\Omega^\perp} \int_{h^k}^{h^{k+1}} \rho g \, v_2 \, dy \, dx$. Combining this with (27) and then with (26) we obtain:

$$-\int_{\Omega^\perp} \int_b^{h^k} \partial_y p \, v_2 \, dy \, dx \approx \int_{\Omega^\perp} \int_b^{h^k} \rho g \, v_2 \, dy \, dx + ...$$
$$+ ... \int_{\Omega^\perp} \int_{h^k}^{h^{k+1}} \rho g \, v_2 \, dy \, dx = \int_{\Omega^\perp} \int_b^{h^{k+1}} \rho g \, v_2 \, dy \, dx. \tag{28}$$

Rewriting the double integration in the equation above back to integration over Ω, and inserting that to the FSSA-stabilized vertical momentum balance (25), we have that:

$$-\int_{\Omega^k} \partial_y p \, v_2 \, d\Omega = \int_{\Omega^k} \rho g \, v_2 \, d\Omega + \Delta t \int_{\partial\Omega^k} (\boldsymbol{u} \cdot \boldsymbol{n}) \, \rho g \, v_2 \, ds$$
$$\approx \int_{\Omega^{k+1}} \rho g \, v_2 \, d\Omega. \tag{29}$$

The left-hand-side integral of (29) is integrated over Ω^k. However, we observe that the addition of the FSSA terms implies that the right-hand-side forcing term of (29) is integrated over Ω^{k+1} in place of Ω^k. Thus, we expect that the solution p from (29) is approximated at time t_{k+1}. When this p is used to compute the velocity in (18) we expect the computed velocities to also be approximated at time t_{k+1}. Using such velocities when advancing the free surface in time through (22) renders an approximately implicit time stepping treatment, which in turn allows taking larger time steps. A more precise observation on this effect is given for the strong form SIA model, which is the focus of the next section.

Stability analysis of SIA combined with FSSA

In the following section, we show how a strong form version of the FSSA terms impacts numerical stability of SIA. The strong setting allows us to derive formulas for the FSSA-stabilized pressure and also for Fourier analysis. We note that the analysis is meant to give a better insight into how FSSA works. The results, however, cannot be directly transferred to the weak setting.

We construct a strong form of FSSA for the strong SIA vertical momentum equation (9). We do that by

starting at the SIA pressure (11) evaluated at t_k, and then adding a scaled normal velocity term, inspired by the FSSA stabilization term in (25). We have:

$$p_*^k = \rho g(y - h^k) - \Delta t\, \rho g\, (\boldsymbol{u} \cdot \boldsymbol{n})|_{y=h^k(x)}. \tag{30}$$

Assuming that the free surface is close to flat we have that $(\partial_x h)^2 \approx 0$ (equivalent to $(\partial_x h)^2 \ll 1$). The surface normal is then $\boldsymbol{n} = (-\partial_x h, 1)/\sqrt{(\partial_x h)^2 + 1^2} \approx (-\partial_x h, 1)$. Using this in (30) we have:

$$p_*^k \approx \rho g\,(y - h^k) - \Delta t\, \rho g\,(-u_{1,s}\, \partial_x h + u_{2,s}). \tag{31}$$

Using (22) on the second term of the right-hand-side of equation above, we arrive at:

$$\begin{aligned} p_*^k &\approx \rho g\,(y - h^k) - \rho g\,(h^{k+1} - h^k) \\ &= \rho g\,(y - h^k + h^k - h^{k+1}) = \rho g\,(y - h^{k+1}) = p^{k+1}. \end{aligned} \tag{32}$$

Hence, the FSSA-inspired correction to the SIA pressure in (30) contributes to approximating pressure at time t^{k+1}. In Appendix we perform the Fourier analysis to show that when using p^{k+1} to compute the strong SIA velocities (i.e. using an implicit representation of the pressure) is enough to alleviate the quadratic time step restriction $\Delta t < C \Delta x^2$ when solving the free surface equation. To derive this result we extended the Von Neumann type analysis for a slab on a slope test case from (Cheng and others, 2017). In (Cheng and others, 2017) the authors show that, assuming thick ice with low surface inclination, the quadratic dependence on Δx is:

$$\Delta t < \frac{3}{5} A_0 |\rho g|^3 C_\alpha^2 \bar{H}^5 (\Delta x)^2, \tag{33}$$

where C_α is the average surface slope and H the ice thickness. The result stems from that the vertical velocity u_2 contains a second derivative of the surface $\partial_{xx} h$. Furthermore, the second derivative of the surface origins from the vertical velocity is a function of $\partial_x u_1$ which is in turn a function of the horizontal pressure derivative $\partial_x p = \rho g\, \partial_x h^k$. Following the derivation of the compact form free surface equation (16) with the coefficients (17), we now write the time discretized free surface equation when assuming that the velocities are derived from p^{k+1}, but that the intermediate integration steps involve h^k. We have:

$$h^{k+1} = h^k + C_0\, \partial_x h^k + C_1\, \partial_x h^{k+1} + C_2\, \partial_{xx} h^{k+1} \tag{34}$$

where:

$$C_0 = \frac{1}{2}A_0(\rho g)^3 \left(-3(b-h^k)^4(\partial_x h^{k+1})^3\right)$$

$$C_1 = \frac{1}{2}A_0(\rho g)^3 \Big((b-h^k)^4 \left(\partial_x h^{k+1}\right)^3 + ... $$

$$+ 4(b-h^k)^4 \, \partial_x b \, \partial_x h^{k+1}\Big) \tag{35}$$

$$C_2 = \frac{1}{2}A_0 \, (\rho g)^3 \Big(-\frac{3}{5}(b-h^k)^5 \left(\partial_x h^{k+1}\right)^2 + ...$$

$$+ 3(b-h^k)^5 \left(\partial_x h^{k+1}\right)^2\Big).$$

We now have an implicit treatment of the leading diffusive $\partial_{xx}h$ term in (34) which leads to a linear time step constraint:

$$\Delta t \le \left(\frac{3}{2}A_0|\rho g|^3 C_\alpha^3 \bar{H}^4\right)^{-1} \Delta x, \tag{36}$$

where C_α is the average surface slope. We derive the above time step restriction for the slab on a slope with a perturbed ice surface case in Appendix and validate the estimate numerically for W-SIA and W-SIAStokes in the numerical experiments section.

COMPUTATIONAL COST ESTIMATION FOR THE DIFFERENT SIA / STOKES FORMULATIONS

The computational work when solving momentum balance models is highly dependent on both software and hardware. However, it is still possible to make estimates of the computational cost, for instance a type of performance analysis approach of (Bueler, 2023). In this section we make rough estimates of the computational cost for ice sheet simulations, where the velocity functions are computed using SIA (9), W-SIA (18), W-SIAStokes (19), W-Stokes (7), and the ice surface is advanced from time t_k to time t_{k+1}, $k = 1, .., N_{\Delta t}$, using the discretized free-surface equation (22). We write the approximate computational cost on the form:

$$\text{Computational cost} = C(d, \alpha) \, C_S \, m^{1+\gamma/(d-1)+\alpha},$$

where:

m is the number of mesh vertices (nodes) in the horizontal direction,

$\alpha \in [0, 2]$ denotes the choice of a linear solver ($\alpha = 2$ dense direct solver, $\alpha = 1$ sparse direct solver, $\alpha = 0.05$ algebraic multigrid solver (Bueler, 2023)). For pure SIA no linear solver is needed and

$\alpha = 0$.

γ is the scaling exponent in the simulation time step restriction $\Delta t \leq C_t \Delta x^\gamma$, where Δx is the horizontal internodal distance.

C_S is a constant specific to the computational cost of the nonlinear Stokes problem which involves the nonlinear iteration count and the choice of hardware,

$C(d, \alpha)$ is a constant depending on α and d, where d is the dimension count of the considered ice sheet geometry.

Following (Bueler, 2023) we have that W-Stokes requires $C_S\, m^{1+\alpha}$ floating point operations until convergence per one time step.

In the W-SIAStokes case the computational cost is the same as in W-Stokes, but divided by the nonlinear iteration count N_{iter}. The cost is $\frac{1}{N_{\text{iter}}}\, C_S\, m^{1+\alpha}$. This is due to that W-SIAStokes only differs from W-SIA in the choice of the viscosity function (linear) (13) and thus requires one iteration to be solved. When making the estimate we also assumed that the different viscosity function preserves the preconditioning quality.

When W-SIA (18) is not FSSA stabilized then the three ($d + 1$ equations in general) equations are solved one by one, and so, in this case, $m \to \frac{m}{d+1}$. This gives the estimate $\frac{d+1}{(d+1)^{1+\alpha}}\, \frac{1}{N_{\text{iter}}}\, C_S\, m^{1+\alpha}$. When W-SIA is FSSA stabilized then the decoupled solution procedure is not possible to perform anymore and the computational cost is the same as in the W-SIAStokes case, that is, $\frac{1}{N_{\text{iter}}}\, C_S\, m^{1+\alpha}$.

Computing the SIA velocities by means of the closed-form expressions (9) requires $C_{\text{SIA}}\, m$ floating point operations.

The computational cost for advancing the ice surface from the initial state to time $t = T$ is proportional to the number of time steps $N_{\Delta t}$ we take along the way. The number of time steps itself is given by $N_{\Delta t} = \frac{T}{\Delta t} \sim \frac{1}{\Delta t}$. For a time step restriction on the form $\Delta t \leq C_t \Delta x^\gamma$, we have that $N_{\Delta t} \sim \frac{1}{\Delta x^\gamma} \sim m^{\gamma/(d-1)}$.

We now combine the computational cost estimates for obtaining the velocity functions, with the computational cost estimate for advancing the ice surface in time. The estimates for all the considered formulations are gathered in Table 1. All the parameters to evaluate the computational costs in the above table are known, except for the time step restriction exponent γ in the case of some SIA formulations. We numerically compute the exponents γ in Section , and then compare the computational cost across the different formulations.

Model	Computational cost estimate
W-Stokes	$C_S\, m^{1+\gamma/(d-1)+\alpha}$
W-Stokes-FSSA	$C_S\, m^{1+\gamma/(d-1)+\alpha}$
W-SIAStokes	$\frac{1}{N_{\text{iter}}}\, C_S\, m^{1+\gamma/(d-1)+\alpha}$
W-SIAStokes-FSSA	$\frac{1}{N_{\text{iter}}}\, C_S\, m^{1+\gamma/(d-1)+\alpha}$
W-SIA	$\frac{d+1}{(d+1)^{1+\alpha}}\, \frac{1}{N_{\text{iter}}}\, C_S\, m^{1+\gamma/(d-1)+\alpha}$
W-SIA-FSSA	$\frac{1}{N_{\text{iter}}}\, C_S\, m^{1+\gamma/(d-1)+\alpha}$
SIA	$C_{\text{SIA}}\, m^{1+\gamma/(d-1)}$

Table 1. Computational cost estimates for obtaining the numerical solutions to a set of considered models. Here, m is the number of mesh vertices in the horizontal direction, d is the number of dimensions, α denotes the choice of a linear solver, γ is the time-step vs. mesh size scaling exponent, C_S is a constant, related to the choice of the nonlinear solver, that scales the number of nonlinear iterations used to solve the reference nonlinear Stokes problem (W-Stokes), and N_{iter} is the number of iterations to solve W-Stokes.

NUMERICAL STUDY

In this section we solve: SIA (9), W-SIA (18), and W-SIAStokes(19). We numerically compute the largest stable time step size Δt when the free surface of an ice sheet is advected in time as described in Section . We find the dependence between Δt and the horizontal mesh size Δx (the CFL condition), compare the errors of the different SIA solutions to the nonlinear Stokes solution and relate them to runtimes. We do this for three different geometries. The experiments are performed by using the FEniCS 2019 library (Alnæs and others, 2014, 2015) on a laptop with the AMD Ryzen 7 PRO 6850U processor and 16 GB RAM.

An algorithm for computing the largest feasible time step when solving the free surface equation

In this section we provide the criterion which we use to numerically compute the largest feasible time step Δt_* when updating the ice sheet surface in time using the free surface equation (1) over domain $\Omega^\perp$ as defined in the scope of Section . Courant-Friedrich-Levy (CFL) condition limits Δt_* in terms of the mesh size Δx:

$$\Delta t_* = C \min_{x_i \in \Omega^\perp} (\Delta x)^p,\ p > 0, \tag{37}$$

where $C > 0$ is the CFL number depending on the type of the discretization of (1) and the data in (1), and the mesh size is:

$$\Delta x = \min_{(x_i \neq x_j) \in \Omega_h^\perp} \|x_i - x_j\|_2, \tag{38}$$

We are interested in the exponent p from (37), where the severity of the time step restriction increases with an increased p, whereas $p = 0$ implies no dependence of Δt_* on Δx. To compute Δt_* numerically we use the stability criterion:

$$\int_{\Omega^\perp} (h(x, t_{k+1}))^2 \, d\Omega^\perp - \int_{\Omega^\perp} (h(x, t_k))^2 \, d\Omega^\perp \leq 0, \ k = 1, 2, .. \tag{39}$$

which has to hold for each time $t_k < T$, where $k = 1, 2, 3, ...$ The above stability criterion measures the difference in the energy of the free surface function across two consecutive time samples. The relation between (39) and the Von Neumann analysis is the following. Within the Von Neumann analysis, the surface function is written as $h(x, t_k) = \sum_{j=-M}^{M} \delta_j(t_k) \, e^{iw_j x}$, where $w_j = \frac{2\pi j}{|P|}$ are wavenumbers, $|P|$ is the domain (interval) size, and $\delta_j^k = \frac{1}{|P|} \int_P h(x, t_k) \, e^{-iw_j x} \, dx$ are the Fourier coefficients. The final statement of the Von Neumann analysis is that there exists $\Delta t > 0$ such that:

$$|\delta_j^{k+1}| \leq |\delta_j^k|.$$

Thus, $\sum_{j=1}^{N} |\delta_j^{k+1}| \leq \sum_{j=1}^{N} |\delta_j^k|$, and using Parseval's identity $\sum_{j=1}^{N} |\delta_j^k| = \int_{-L}^{L} h(x, t)^2 \, d\Omega^\perp$ on each side of the inequality, and then moving the right-hand-side term to the left-hand-side we obtain (39). We pose the computation of Δt_* as the following optimization problem. Find $\max \Delta t_*$ subject to:

$$\int_{\Omega^\perp} (h(x, t_{k+1}))^2 \, d\Omega^\perp - \int_{\Omega^\perp} (h(x, t_k))^2 \, d\Omega^\perp < 0,$$
$$k = 1, 2, ..., N_T, \tag{40}$$

where $\int_{\Omega^\perp} (h(x, t_{k+1}))^2 \, d\Omega^\perp$ and $\int_{\Omega^\perp} (h(x, t_k))^2 \, d\Omega^\perp$ are the free-surface energies evaluated in two consecutive time steps, and N_T is the number of time steps to perform the simulations in time $t \in (0, T]$. The stability criterion (40) applies to simulations where the physical (exact) surface energy does not grow in time.

To understand how Δt_* depends on Δx, we discretize (1) using different mesh sizes $(\Delta x)_j$, $j = 1, 2, ..,$ and then for each $(\Delta x)_j$ compute $(\Delta t_*)_j$ by solving one optimization problem (40). We solve the opti-

Slab on a slope surface case

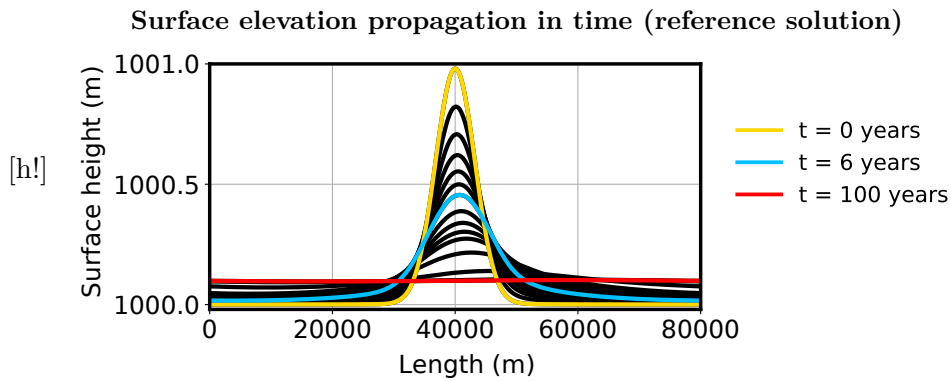### Surface elevation propagation in time (reference solution)

Fig. 2. Propagation of the surface elevation function in time when computed as a solution to the nonlinear Stokes problem (reference), where the simulation time step is $\Delta t = 0.1$ years. Horizontal mesh size and vertical mesh size are $\Delta x = 250$ m and $\Delta y = 90$ m respectively.

mization problem using the bisection method. Once all the data paris $((\Delta x_*)_j, \Delta t_*)_j)$, $j = 1, 2, ...$, are known, we approximate the exponent p in (37) by fitting a linear function to the transformed data pairs $((\log_{10} \Delta x_*)_j, (\log_{10} \Delta t_*)_j)$, $j = 1, 2, ...$, where p takes the value of the slope of the fitted linear function. Note that this is a fairly computationally expensive procedure, which is the reason why we restrict ourselves to two dimensions in this study.

Slab on a slope with perturbed surface

Configuration

First, we run experiments for a slab on a slope with a perturbed surface, as this is the setting of the von Neumann analysis in (). The ice sheet is a two-dimensional slab, $L = 80 \times 10^3$ m long, and $H = 1 \times 10^3$ m thick, inclined with $\alpha = 0.75$ degrees measured in the clockwise direction, with the initial surface:

$$h(x, 0) = H + e^{-5 \times 10^{-8}(x - \frac{L}{2})^2}.$$

For the free-surface equation (1) we impose periodic boundary conditions (2) as this is required for the von Neumann analysis. We impose no-slip boundary conditions on Γ_b, stress-free boundary conditions on Γ_s, and periodic boundary conditions on Γ_l.

The relation between the number of discretization points in the horizontal direction $n_x = m$ and Δx that

Slab on a slope surface case

Number of elements and the mesh size

n_x	20	30	40	50	60	70	80	120	160	200
Δx	4000.0	2666.7	2000.0	1600.0	1333.3	1142.9	1000.0	666.7	500.0	400.0

n_x	240	280	320	480	640	1000	1280	1560	1800	
Δx	333.3	285.7	250.0	166.7	125.0	80.0	62.5	51.3	44.4	

Table 2. Number of the discretization points in the horizontal direction n_x and the corresponding horizontal mesh size Δx for the Slab on a slope surface case.

we use to perform the experiments is given in Table 2. Note that $n_y = 11$ (corresponding to $\Delta y = 90$ m) is fixed for all experiments and the FSSA scaling parameter is fixed at $\theta = 1$, unless stated otherwise.

Accuracy

In Figure 2 we show how the perturbed surface evolves in time, where the final simulation time is $t = 100$ years. Here the solution is computed using the nonlinear Stokes problem which we consider a reference, with a small time step $\Delta t = 0.1$ years, the horizontal mesh size $\Delta x = 250$ m and the vertical mesh size $\Delta y = 90$ m. In Figure 3 we plot the solutions of the different SIA problem formulations to the reference solution, where all the solutions are evaluated at $t = 6$ years. We observe that all the solutions are close to the reference solution. The solution to W-SIAStokes appears overall closest to the reference. The addition of the FSSA stabilization term increases the error, but not significantly.

Time step restriction scaling

Now we compute Δt_* as a function of Δx as described in Section . We run the simulations with and without the FSSA terms defined in the scope of Section . The final simulation times are adjusted to the magnitude of the largest time step sizes making the comparison more realistic. We use the final simulation times: $t = 100$ years (W-SIAStokes-FSSA and W-SIA-FSSA), $t = 12$ years (W-SIAStokes and W-SIA), $t = 5$ years (SIA). The results are shown in the first plot of Figure 4. We observe that the largest stable time step Δt_* is allowed to be from 10 times (coarse resolution) to 100 times (fine resolution) larger when using W-SIAStokes as compared to W-SIA. Furthermore, in W-SIAStokes, Δt_* has a constant relation to Δx over the whole range of the chosen Δx except for the finest resolution where the relation becomes

Slab on a slope surface case

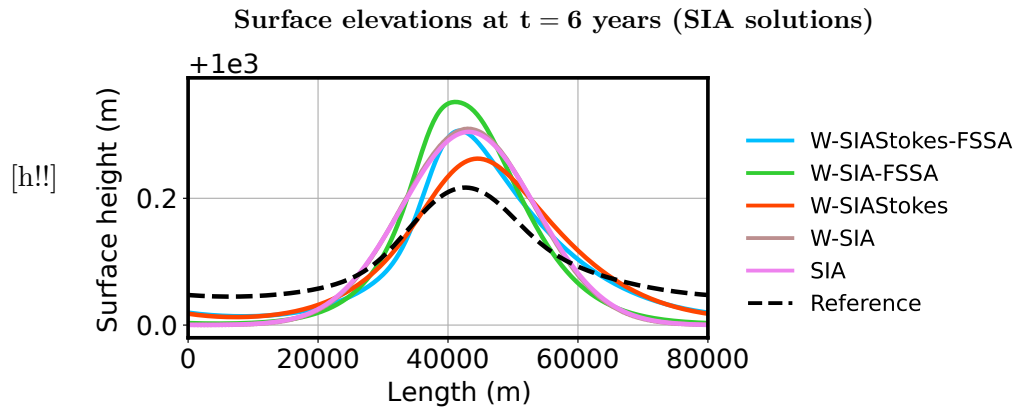**Surface elevations at t = 6 years (SIA solutions)**

Fig. 3. Surface elevations at simulation time $t = 6$ years for different SIA problem formulations and the reference formulation (nonlinear Stokes problem). Horizontal and vertical mesh sizes are $\Delta x = 250$ m and $\Delta y = 90$ m respectively. The largest feasible time step Δt_* for the given Δx and Δy is chosen for each formulation: $\Delta t_* = 6$ years, $\Delta t_* = 12$ years, $\Delta t_* = 1.8$ years, $\Delta t_* = 0.04$ years, $\Delta t_* = 0.008$ years, $\Delta t = 0.1$ years for (W-SIAStokes-FSSA), (W-SIA-FSSA), (W-SIAStokes), (W-SIA), (SIA), (Reference) respectively.

Slab on a slope surface case

(a)   **(b)**
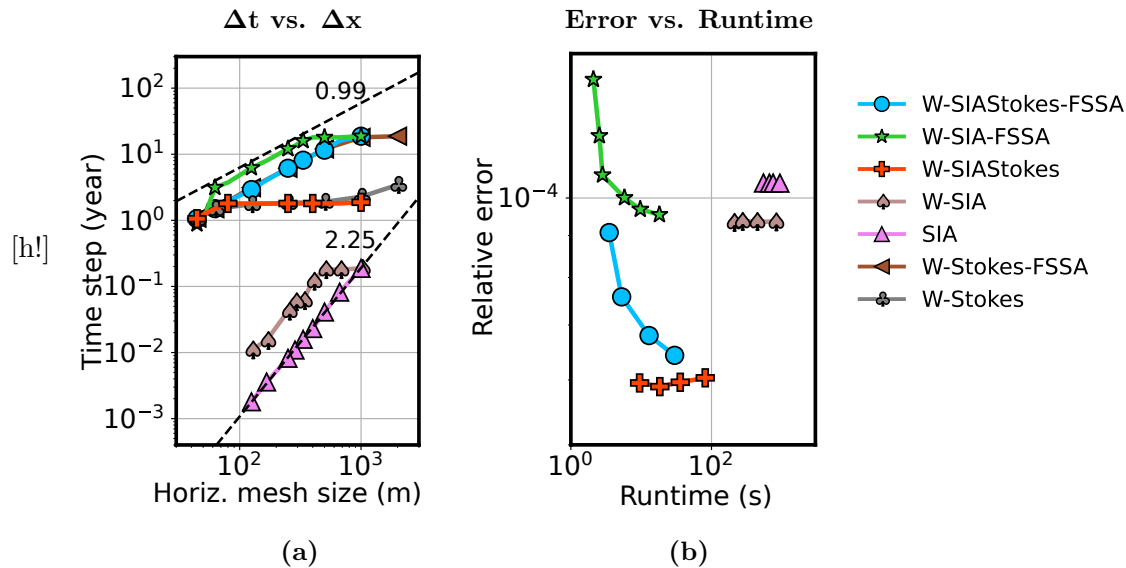
Fig. 4. (a) Scaling of the largest feasible time step Δt_* as a function of the horizontal mesh size Δx when the vertical mesh size $\Delta y = 90$ m is fixed. (b) The model error as a function of the wall clock runtime when the nonlinear Stokes solution is taken as a reference. In all cases, the final time is fixed at $t = 20$ years. Mesh sizes $\Delta x = 250$ m and $\Delta y = 90$ m are also fixed. The time step is refined starting at the formulation largest feasible time step $\Delta t = \Delta t_*, \Delta t_*/2, \Delta t_*/4, ...$ The time step for the reference solution is fixed at $\Delta t = 0.1$ years.

linear. The allowed time steps when using SIA and W-SIAStokes are small. The $\Delta_* t$ vs. Δx scaling in the latter two formulations is quadratic which is less desired.

Run-time versus accuracy

Next, we perform an experiment measuring the ratio between the relative model error and the computational (wall clock) runtime for each of the SIA formulations. This is important as a small Δt does not necessarily imply a small computational time for the whole simulation. This depends on the computational time required to evaluate the velocity functions in each time step. We set the final simulation time to $t = 20$ years. For W-SIAStokes-FSSA we used $\Delta t = 6, 3, 1.5, 0.75$. For W-SIA-FSSA we used $\Delta t = 12, 6, 3, 1.5, 0.75, 0.4$. For W-SIAStokes we used $\Delta t = 1.8, 0.9, 0.45, 0.2$. For W-SIA we used $\Delta t = 0.04, 0.03, 0.02, 0.01$, and for SIA we used $\Delta t = 0.008, 0.007, 0.006, 0.005$. The error is computed with the nonlinear Stokes solution as a reference with $\Delta t = 0.1$ years. In all cases the mesh sizes $\Delta x = 250$ m and $\Delta y = 90$ m are fixed. The result is given in the second plot of Figure 4. We observe that W-SIAStokes-FSSA allows small computational runtimes with only a mild increase in the model error. W-SIA-FSSA also allows for small computational runtimes, but the model error is larger than in the W-SIAStokes-FSSA case. The unstabilized (weak nor strong) SIA formulations do not allow for small computational runtimes, except in the case when we use the W-SIAStokes formulation.

Impact of the FSSA parameter θ on the time step restriction scaling

As we demonstrated in the previous paragraphs W-SIAStokes-FSSA allows for the largest time steps among all the considered formulations. The FSSA parameter in those experiments was fixed at $\theta = 1$. In Figure 5 we illustrate the effect of the choice of θ on the scaling of the largest feasible time step Δt_* as a function of Δx. We observe that choice of small θ leads to a non-robust Δt_* vs. Δx scaling behaviour, where Δt_* has to be taken around 10-times smaller as $\theta \to 0$. As the FSSA parameter approaches $\theta = 0.2$ then the Δt_* vs. Δx scaling approaches the linear behaviour as also observed in Figure 4. Furthermore, the scaling stays the same for $\theta > 0.2$. This implies that, for the given test case, the choice of θ is not sensitive, and can be left at $\theta = 1$ without losing the length of the largest feasible time step.

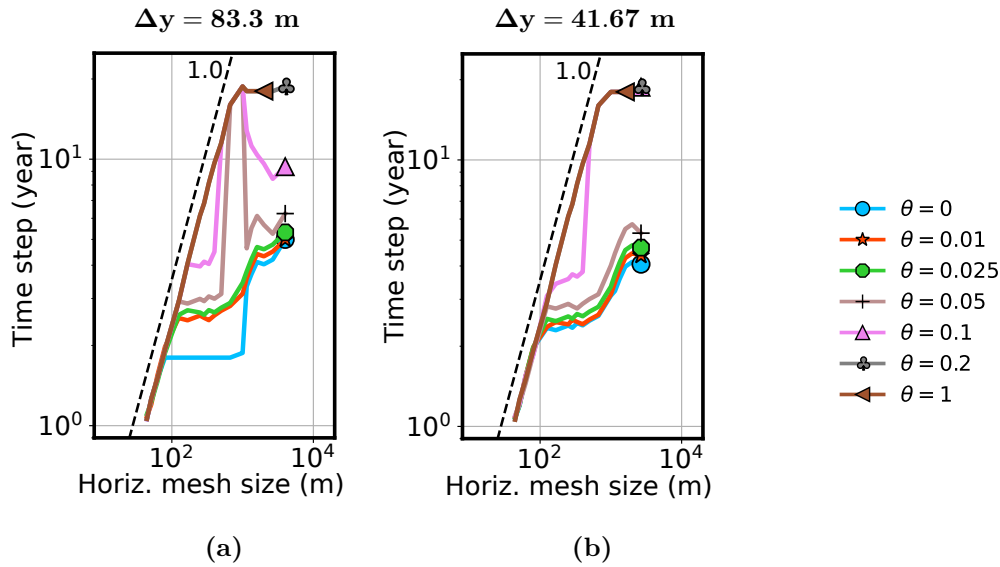**Slab on a slope surface case, varying θ (FSSA parameter), W-SIAStokes-FSSA**

Fig. 5. Largest feasible time step Δt_* as a function of the horizontal mesh size Δx for the W-SIAStokes-FSSA formulation, when the FSSA parameter θ varies. Vertical mesh size is fixed at $\Delta y = 83.3$ m in (a), and at $\Delta y = 41.67$ m in (b).

An idealized ice sheet surface case

Configuration

We now change the configuration to study the impact of ice sheet margins. The ice sheet configuration in this test case takes horizontal values $x \in [-L, L]$ and vertical values $y \in [0, H]$, where the ice sheet half half-length is $L = 750 \times 10^3$ m and the ice sheet height is $H = 3 \times 10^3$ m. To construct the ice sheet surface for this test case we define the following auxiliary profile:

$$h_1(x) = \left(3 - \left(\frac{x}{L} \right)^2 \right)^{0.58},$$

and then use it in the initial surface definition:

$$h(x, 0) = H \frac{h_1(x) - h_1(-L)}{h_1(0)}.$$

When solving the free-surface equation (1) we set Dirichlet boundary conditions $h(-L, t) = h(-L, 0)$ on the left boundary, and $h(L, t) = h(L, 0)$ on the right boundary. When solving one of the momentum

An idealized ice sheet surface case

Number of elements and the mesh size

$\mathbf{n_x}$	80	200	400	600	800	1000
$\mathbf{\Delta x}$	18750	7500	3750	2500	1875	1500

Table 3. Number of the discretization points in the horizontal direction n_x and the corresponding horizontal mesh size Δx for the idealized ice sheet surface case.

balances we impose no-slip boundary conditions on Γ_b and Γ_l, whereas on Γ_s we set stress-free boundary conditions.

The relation between the number of horizontal mesh elements n_x and horizontal mesh size Δx that we use to perform the experiments is given in Table 3 below.

Note that the number of vertical mesh elements is $n_y = 12$ (corresponding to vertical mesh size $\Delta y = 250$ m) and is fixed for all experiments unless stated otherwise. The FSSA scaling parameter is always fixed at $\theta = 1$.

Time step restriction scaling

In the left plot of Figure 6 we display the largest feasible time step Δt_* as a function of Δx for the different SIA formulations. Time step Δt_* scales linearly with respect to Δx for W-SIAStokes and W-SIAStokes-FSSA. For SIA and W-SIA we observe a quadratic scaling. The benefits when using the FSSA stabilization terms together with W-SIA disappear as the Δx is fine enough. Among all the formulations the largest time steps can be taken when W-SIAStokes W-SIAStokes-FSSA are used. For W-SIAStokes-FSSA the time steps increase approximately 100 times, across the whole range of the considered mesh sizes. In the W-SIAStokes case the addition of the FSSA stabilization terms allows for a significantly smaller computational time but gives rise to a (typically small) increase in the approximation error.

Run-time versus accuracy

In the next experiment, we compute the ratio between the computational runtime (wall clock) and the modelling error. For all formulations, we fixed the horizontal mesh size to $\Delta x = 3750$ m and ran the simulation until $t = 100$ years. The error is computed using the nonlinear Stokes solution as a reference, where the time step is $\Delta t = 0.1$ years. The maximum time steps for testing each SIA formulation is taken

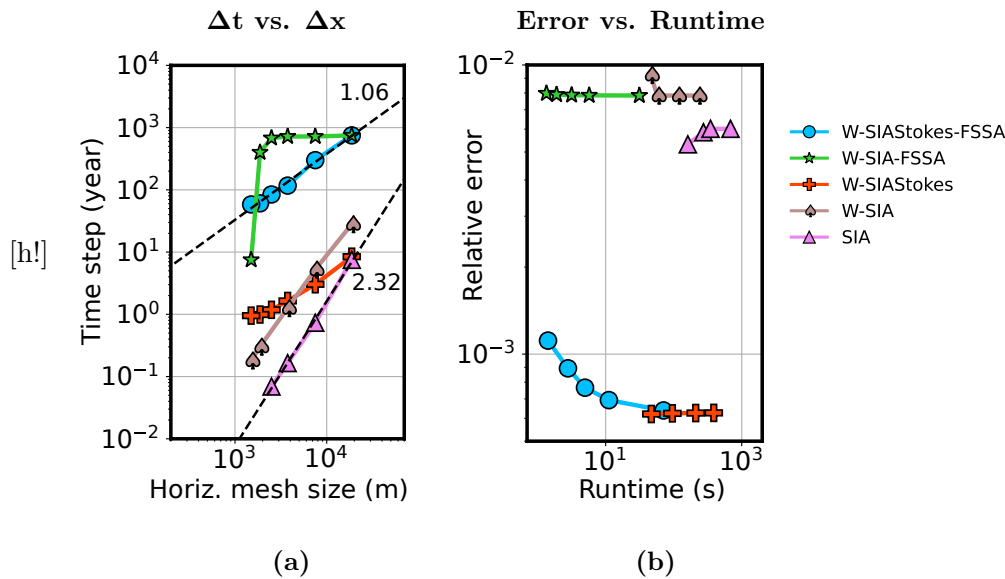## An idealized ice sheet surface case

Fig. 6. (a) scaling of the largest feasible time step Δt_* as a function of the horizontal mesh size Δx when the vertical mesh size $\Delta y = 90$ m is fixed. (b) the model error as a function of the wall clock runtime when the nonlinear Stokes solution is taken as a reference. In all cases the final time is fixed at $t = 20$ years. Mesh sizes $\Delta x = 250$ m and $\Delta y = 90$ m are also fixed.

in line with the largest feasible time step for $\Delta x = 3750$ m from Figure 6. For both FSSA stabilized weak SIA formulations we used $\Delta t = 50, 25, 12.5, 6, 1$. For W-SIAStokes we used $\Delta t = 1.6, 0.8, 0.4, 0.2$. For W-SIA we used $\Delta t = 1, 0.8, 0.4, 0.2$, and for SIA we used $\Delta t = 0.16, 0.1, 0.08, 0.04$. The results are presented in Figure 6, plot on the right. Runtime vs. error ratio of W-SIASTokes is favourable over all the other formulations that we consider. This is, both, when the FSSA terms are present, and when the FSSA terms are not present.

Long time simulations

We now compute the surface evolution over a long period: the final time is $t = 10^4$ years. We choose a fine mesh size $\Delta x = 1500$ m. The time step is chosen in line with Figure 6 (left plot) for the given Δx, that is, $\Delta t = 58.2$ years for W-SIAStokes, and $\Delta t = 7.5$ years for W-SIA. In Figure 7 we show the solutions obtained from the two formulations. The solution obtained using W-SIAStokes does not entail any oscillations, whereas the solution in the W-SIA case entails oscillations close to the lateral boundaries. We have not fully explored the behaviour. However, we speculate that this is due to the lack of control

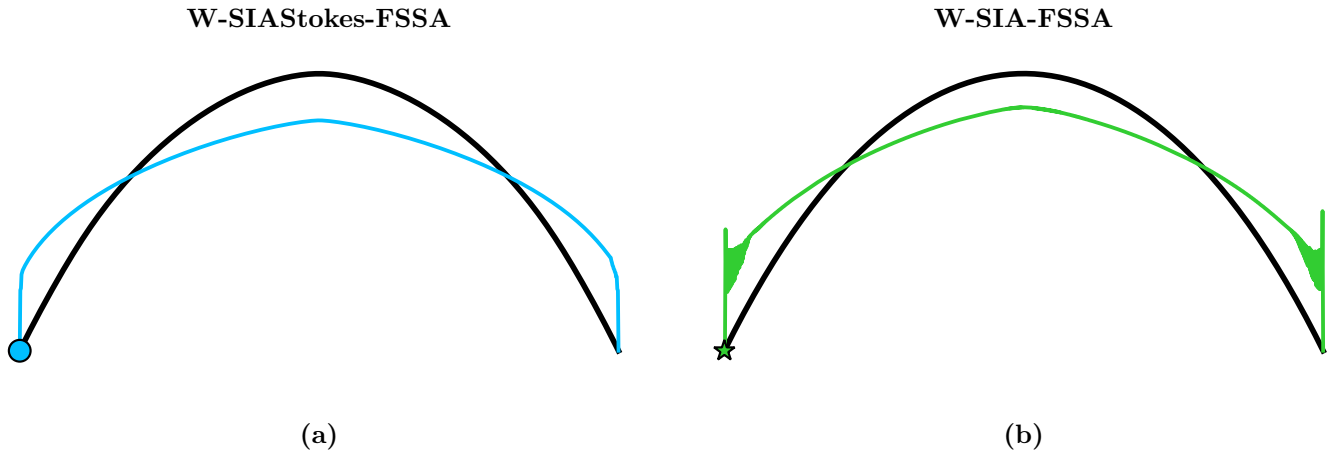**[h!]**

Idealized ice sheet surface case

Surface elevations at $\mathbf{t} = \mathbf{10^4}$ years

W-SIAStokes-FSSA   **W-SIA-FSSA**

(a)   **(b)**

Fig. 7.   Two surface evolutions after $t = 10^4$ years. The horizontal mesh size is $\Delta x = 1500$ m, whereas the vertical mesh size is $\Delta y = 250$ m. The time steps take the largest feasible values for the given mesh sizes: $\Delta t = 58.2$ years for W-SIAStokes in (a), and $\Delta t = 7.5$ years for W-SIA in (b). Both formulations are stabilized using the FSSA stabilization terms with the FSSA parameter set to $\theta = 1$.

over all strain components in W-SIA (see 18) in contrast with W-SIAStokes (19), where all the strain components are present. This implies that a bound $\|\boldsymbol{Du}\|_{L^2(\Omega)} \leq \|\boldsymbol{f}\|_{L^2(\Omega)}$, where $\boldsymbol{f}$ is the gravity field, can be obtained by using Korn's inequality. This provides control over the derivatives of the velocities $\boldsymbol{u}$, which prevents $\boldsymbol{u}$ from being too oscillatory.

A two-dimensional cross-section of Greenland

Configuration

In this test case, we still consider a two-dimensional ice sheet geometry, but with a more realistic initial surface elevation as well as a more realistic bedrock elevation. We simplify the full three-dimensional Greenland geometry obtained from BedMachine Morlighem and others (2017), and intersect it with a horizontal line to get the boundary points over a cross section as displayed in Figure 8. Then we represent the surface elevation and the bedrock elevation by using a cubic spline interpolation. This allows for evaluating the surfaces at an arbitrary location, which we employ when considering horizontally varying mesh sizes in our computational study.

Greenland (2D) profile case

Number of elements and the mesh size

n_x	80	200	400	600	800	1000
Δx	12362	4945	2472	1648	1236	989

Table 4. Number of the discretization points in the horizontal direction n_x and the corresponding horizontal mesh size Δx for the Greenland (2D) profile case.
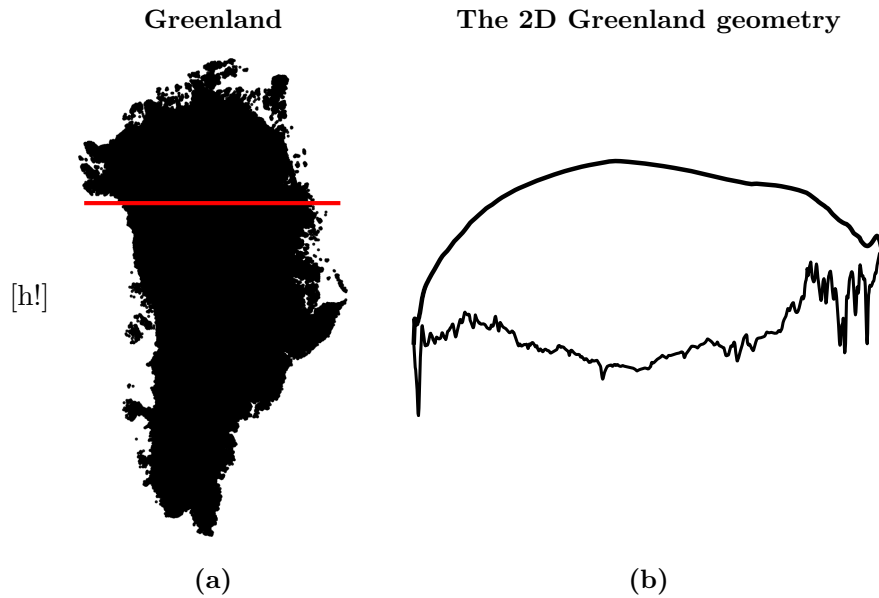
Greenland   **The 2D Greenland geometry**

[h!]

(a)   (b)

Fig. 8. Top view over a three-dimensional Greenland geometry Morlighem and others (2017) (a), where the intersecting red line gives the boundary of the Greenland cross-section (b) used as one of the computational domains in this paper.

When solving the free-surface equation (1) we set Dirichlet boundary conditions $h(-L, t) = h(-L, 0)$ on the left boundary, and $h(L, t) = h(L, 0)$ on the right boundary. When solving one of the momentum balances we impose no-slip boundary conditions on Γ_b and Γ_l, whereas on Γ_s we set stress-free boundary conditions.

The relation between the number of horizontal mesh elements n_x and horizontal mesh size Δx that we use to perform the experiments is given in Table 4.
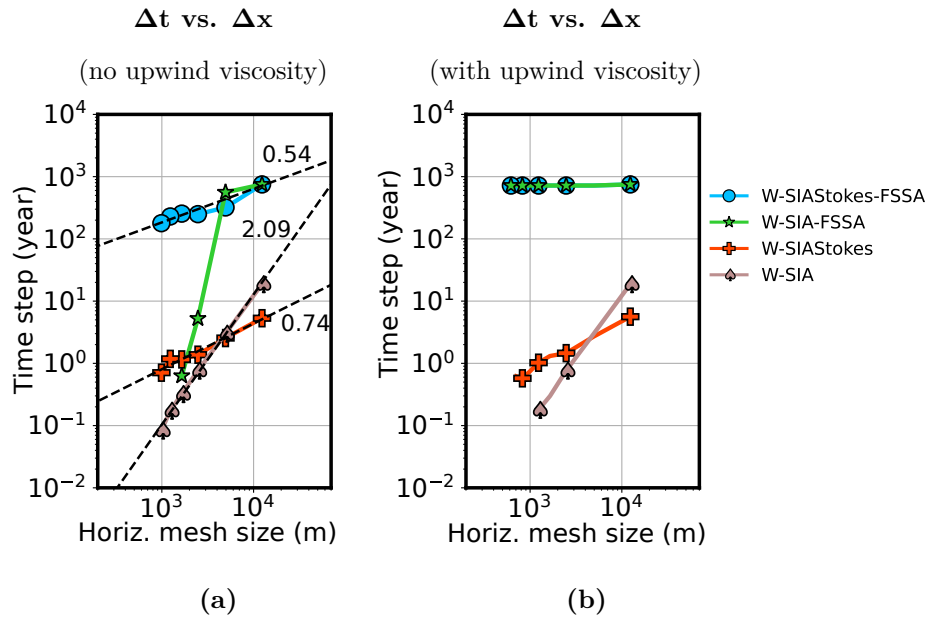
Greenland (2D) surface case

Fig. 9. (a) Scaling of the largest feasible time step Δt_* as a function of the horizontal mesh size Δx when the vertical mesh size is fixed. (b) The model error as a function of the wall clock runtime when the nonlinear Stokes solution is taken as a reference. In all cases, the final time is fixed at $t = 400$ years. The horizontal mesh size is fixed at $\Delta x = 2472$ m.

Time step restriction scaling

In Figure 9 (left plot) we investigate the scaling of Δt as a function of Δx. We observe that in the case of W-SIAStokes, the order of scaling is approximately 0.75, whereas in the W-SIAStokes-FSSA case, the order of scaling is close to 0.5. The scaling in the W-SIA case is approximately of order 2, which is similar as in all previous test cases. When W-SIA-FSSA is used the scaling behaves unpredictably, similar as in Section . Among all the formulations, the time steps are the largest in the W-SIAStokes-FSSA.

Upwinding

After visualizing the computed solutions using all the considered SIA formulations we observed spurious oscillations over the western part of the two-dimensional Greenland geometry (see Figure 10). For that reason we in addition combined the SIA formulations with the first-order viscosity (also upwind viscosity) operator added to the free-surface equation. The role of that operator is dampening of the spurious oscillations. In Figure 9 (right plot) we compute the scaling of Δt as a function of Δx when the first-order

viscosity operator is added to the free-surface equation, for each of the considered SIA formulations. We observe that the scaling does not change when no FSSA terms are added W-SIAStokes or W-SIA. However, the scaling, when the FSSA terms are employed, changes from linear (no first-order viscosity) to constant (with first-order viscosity). The latter is favourable.

Long time simulations

In Figure 10 we, for each of the considered SIA formulations, plot the surface elevations after $t = 400$ years of simulation time, at $\Delta x = 2472$ m, and make a comparison towards the surface elevations computed using the nonlinear Stokes problem (reference). We observe that all the SIA formulation solutions are overall a good approximation to the reference solution. As stated in the previous paragraph, all solutions in the first three rows of Figure 10 involve spurious oscillation at the western part of the two-dimensional Greenland geometry. The plots in the last row of Figure 10 display the viscous solutions, and we observe that the oscillations have disappeared. Similar behavior is observed for the numerical solutions when $t = 10000$ years in Figure 12

Run-time versus accuracy

In Figure 11 compute the ratio between the computational runtime (wall clock) and the modelling error. For all formulations, we fixed the horizontal mesh size to $\Delta x = 2472$ meters, and ran the simulation until $t = 400$ years. The error is computed using the nonlinear Stokes solution as a reference, where the time step is $\Delta t = 0.4$ years. The maximum time steps for testing each SIA formulation is taken in line with the largest feasible time step for $\Delta x = 2472$ m from Figure 9. For W-SIAStokes-FSSA we used $\Delta t = 249, 125, 60, 30, 10, 1, 0.5$ years. For W-SIA-FSSA we used $\Delta t = 5, 2.5, 1, 0.5, 0.4$ years. For W-SIAStokes, we used $\Delta t = 1.37, 0.9, 0.65, 0.4$ years. For W-SIA we used $\Delta t = 0.76, 0.6, 0.5, 0.4$. When W-SIAStokes-FSSA and W-SIA-FSSA are further augmented with the with upwind viscosity in the free-surface equation we used $\Delta t = 800, 400, 200, 100, 50, 25, 12.5$ years. We observe that the FSSA stabilized weak formulations augmented with the upwind viscosity term have by far the best error vs. runtime ratio.

Greenland (2D) surface case

Surface elevation comparison against the reference at t = 400 years

W-SIAStokes-FSSA

W-SIA-FSSA

W-SIAStokes

W-SIA
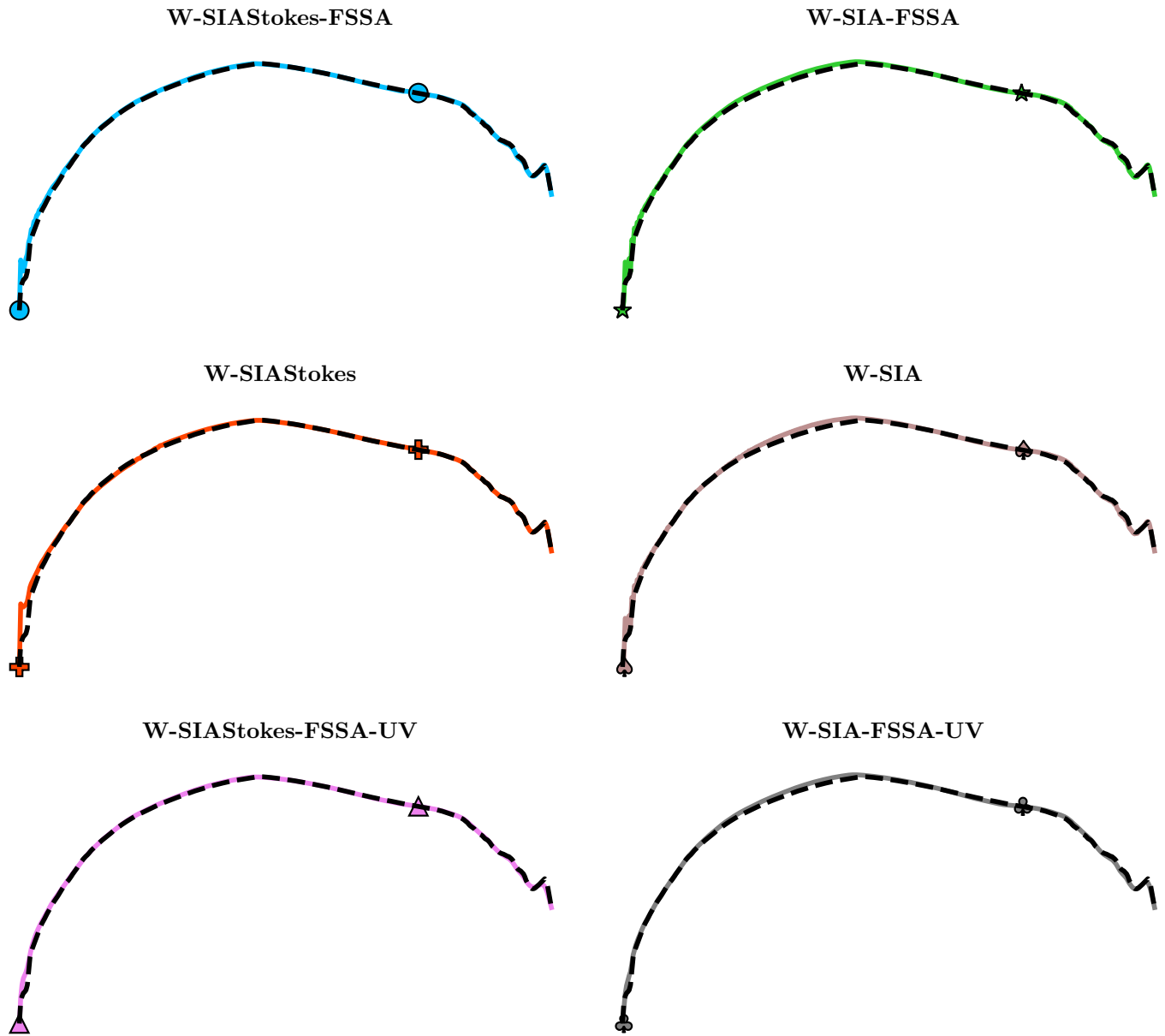
W-SIAStokes-FSSA-UV

W-SIA-FSSA-UV

Fig. 10. Surface evolutions computed using different SIA formulations, after $t = 400$ years. The horizontal mesh size is $\Delta x = 2472$ m. The time steps take the largest feasible values for the given mesh sizes (see Figure 9).
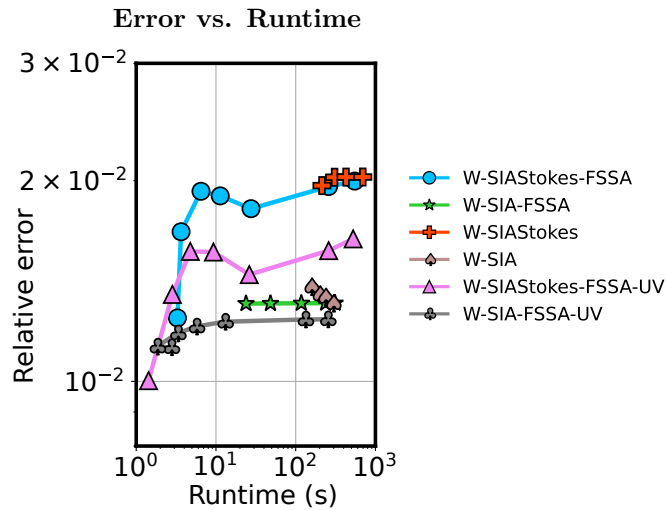
Greenland (2D) surface case

Error vs. Runtime

Fig. 11. Approximate model error as a function of the wall clock runtime when the nonlinear Stokes solution is taken as a reference. In all cases, the final time is fixed at $t = 400$ years. The horizontal mesh size is $\Delta x = 2472$.

Computational cost estimates with the parameters inferred from the numerical experiments

In the subsections above we gathered experimental data on the slope of the scaling of the time step restriction as a function of the horizontal mesh size. In this subsection we use those slopes in place of the parameter γ in , to speculate on the relation between computational work and the number of horizontal mesh nodes m for the different momentum models. Across the experiments, we observe that W-SIA-FSSA, W-SIAStokes, and W-SIAStokes-FSSA have a linear time-step constraint $\gamma = 1$. On Greenland with upwind viscosity, we saw that γ can also be smaller than 1, but we here chose the worst-case scenario value ($\gamma = 1$) for W-SIA-FSSA and W-SIAStokes. In the W-SIA model case, the worst case is $\gamma = 2$. The same holds for the standard SIA model case. We gather these results in Table 5. In the W-Stokes-FSSA case, we get $\gamma = 1$, whereas in the W-Stokes case, we have $\gamma = 1$ when the horizontal mesh size is small, and $\gamma = 0$ for larger horizontal mesh sizes – the worst case is then $\gamma = 1$.

We observe that the SIA model has the lowest asymptotic cost scaling m^2. The next best is W-SIAStokes-FSSA with $m^{2.5}$ when $\alpha = 1$ (sparse direct solver). We argue that the computational cost is in the two cases comparable when it comes to the asymptotic scaling as $m \to \infty$. However, knowing that the SIA model is a crude simplification of the Stokes model (4), and that the W-SIAStokes model only carries minor

Greenland (2D) surface case
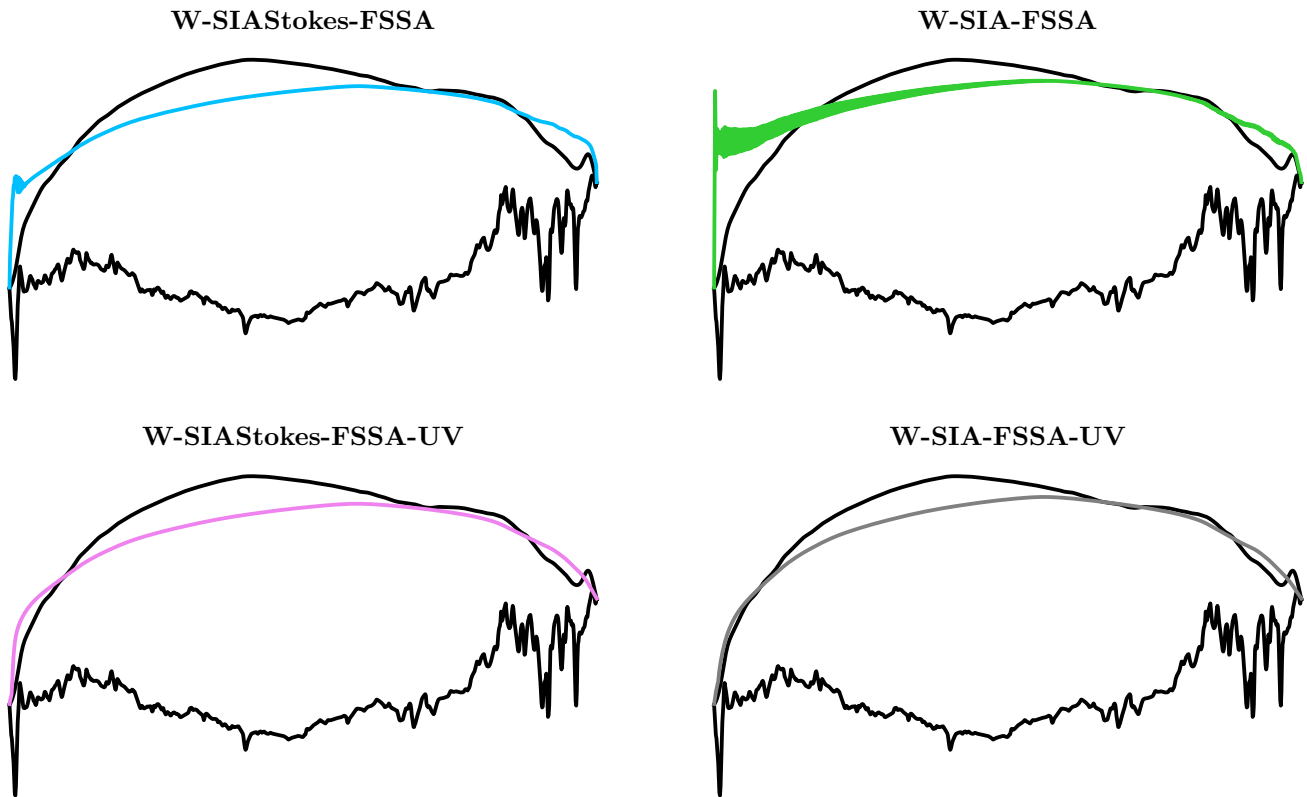
Surface elevations at t = 10000 years

Fig. 12. Surface elevations computed using the FSSA stabilized SIA formulations, with and without the first-order (upwind) viscosity added to the free-surface equation. The surface elevations are evaluated at $t = 10000$ years. The horizontal mesh size is $\Delta x = 2472$ m. The time steps take the largest feasible values for the given mesh sizes (see Figure 9).

Model	γ	Computational cost estimate	Evaluated with γ and d = 3
W-Stokes	1	$C_S\, m^{1+\gamma/(d-1)+\alpha}$	$C_S\, m^{1.5+\alpha}$
W-Stokes-FSSA	1	$C_S\, m^{1+\gamma/(d-1)+\alpha}$	$C_S\, m^{1.5+\alpha}$
W-SIAStokes	1	$\frac{1}{N_{\text{iter}}} C_S\, m^{1+\gamma/(d-1)+\alpha}$	$\frac{1}{N_{\text{iter}}} C_S\, m^{1.5+\alpha}$
W-SIAStokes-FSSA	1	$\frac{1}{N_{\text{iter}}} C_S\, m^{1+\gamma/(d-1)+\alpha}$	$\frac{1}{N_{\text{iter}}} C_S\, m^{1.5+\alpha}$
W-SIA	2ă	$\frac{d+1}{(d+1)^{1+\alpha}} \frac{1}{N_{\text{iter}}} C_S\, m^{1+\gamma/(d-1)+\alpha}$	$\frac{4}{4^{1+\alpha}} \frac{1}{N_{\text{iter}}} C_S\, m^{2+\alpha}$
W-SIA-FSSA	1	$\frac{1}{N_{\text{iter}}} C_S\, m^{1+\gamma/(d-1)+\alpha}$	$\frac{1}{N_{\text{iter}}} C_S\, m^{1.5+\alpha}$
SIA	2	$C_{\text{SIA}}\, m^{1+\gamma/(d-1)}$	$C_{\text{SIA}}\, m^2$

Table 5. Computational cost estimate comparison across the different formulations of the shallow ice approximation (SIA) model, when using the solution (the velocity) to advance the ice sheet surface in time. Here, m is the number of mesh vertices in the horizontal direction, d is the number of dimensions, α denotes the choice of a linear solver, γ is the time-step vs. mesh size scaling exponent, C_S is a constant, related to the choice of the nonlinear solver, that scales the number of nonlinear iterations used to solve the reference nonlinear Stokes problem (W-Stokes), and N_{iter} is the number of iterations to solve W-Stokes.

simplified elements (the viscosity) as compared to W-Stokes, the W-SIAStokes model is more accurate as we could also observe from the runtime vs. error experiments figures. The computational cost in the W-SIA model also scales as $m^{1.5+\alpha}$, but this does not hold for all the horizontal mesh size choices as observed from the experiments. We note that N_{nlin} is large for large Δt. This is due to that the nonlinear iteration initial guess to compute the solution at time t_{k+1} is the solution from time t_k, and the two solutions when $\Delta t = t_{k+1} - t_k$ is large, are typically very different, implying that the nonlinear iteration count is large.

The time step sizes can also be restricted by some other components of an ice sheet model, such as the temperature evolution or climate data. However, when these time step sizes are small, it is still not certain that the velocity solution has to be updated at the same small time step as e.g. the temperature. This study is out of the scope of this paper.

FINAL REMARKS

In this paper, we investigated the benefits when using the SIA momentum balance model (41) written on different weak formulations. We referred to the weak SIA model (18) as W-SIA, the modified weak SIA model alias weak form linear Stokes equations employing the SIA viscosity function as W-SIAStokes, the weak full nonlinear Stokes problem as W-SIA, and to the standard (strong form) SIA model as SIA.

When the different SIA forms were additionally stabilized by mean of the FSSA terms (23) we appended an abbreviation FSSA to each of the form abbreviations.

The key outcomes of the present study are that in the considered test cases:

W-SIA-FSSA allows for large time steps with linear scaling, but limited to coarse Δx.

W-SIAStokes and W-SIAStokes-FSSA have linear time step restriction scaling for all Δx,

W-SIAStokes is numerically more robust and accurate compared to W-SIA for a small cost increase.

We expand on the list above in the paragraphs written below.

The first weak formulation is W-SIA (18). An immediate benefit when using W-SIA is that we were able to add the FSSA stabilization terms (23) (W-SIA-FSSA). This improved the time step restriction from quadratic (W-SIA) to linear (W-SIA-FSSA) scaling in terms of the horizontal mesh size Δx when using the W-SIA velocities for solving the free surface equation. Overall, the time step sizes in all the considered test cases were increased by at least approximately 100-times as compared to the standard SIA formulation time step sizes. However, we observed that when Δx is small enough, the largest time step size behaviour became unpredictable and started taking values similar to the standard SIA time step sizes. We have not experimentally assessed the largest feasible time steps in 3D. However, according to our computational cost estimates, the differences across SIA and W-SIA-FSSA are smaller in 3D.

As a remedy, we modified W-SIA to W-SIAStokes (19) by adding the originally neglected stress terms back to W-SIA, but kept the SIA viscosity (13) intact so that W-SIAStokes remained a linear problem. We observed predictable largest time step size behaviour. The time step scaled linearly in terms of Δx without even adding the FSSA stabilization terms to the weak formulation. After we added the FSSA stabilization terms to W-SIAStokes (W-SIAStokes-FSSA) the scaling remained linear, but the largest time step sizes have in general significantly increased, whereas the approximation error increased only slightly. In one of the tests we compared W-SIAStokes to W-Stokes and found that the time step sizes, including the scaling in terms of Δx, were comparable.

When compared to the standard SIA model, W-SIA and W-SIAStokes models had a smaller error, taking the W-Stokes solution as a reference. This held also when the FSSA stabilization terms were added to the two weak formulations and very long time steps were used. The error vs. runtime ratio was also favourable in the case of both weak formulations (with and without the FSSA stabilization) over the standard SIA solution. Among the two, W-SIAStokes had a better error vs. runtime ratio, (with and

without the FSSA stabilization). We note that the runtime measurements could differ depending on the code implementation of the different SIA formulations.

To view the observed runtime measurements from another angle, we performed a theoretical computational cost estimation in Section . Based on that we conclude that the computational cost of W-SIA and W-SIAStokes is comparable to that of the standard SIA model, in terms of the asymptotic behaviour, that is, when the number of the horizontal mesh vertices is increased.

Throughout the paper we used no-slip boundary conditions for simplicity. The FSSA stabilization terms are effective also when using the moderate slip boundary conditions Löfgren and others (2023).

We anticipate that glaciologists interested in the ice spin-up simulations of which the simulation length is on the order of hundreds of thousands of years could benefit from using the W-SIA-FSSA model or the W-SIAStokes-FSSA model over the standard SIA model. Note that our results are for isothermal simulations. More studies are needed to investigate the time step restrictions related to temperature evolution and other physical processes. However, we believe resolving the restriction due to the velocity-surface coupling is the most difficult problem.

We speculate that the W-SIAStokes model is a good choice to replace the standard SIA model within the scope of coupled models. One of them is the ISCAL (Ice Sheet Coupled Approximation Level) model Ahlkrona and others (2016) where the standard SIA model and the W-Stokes model are used dynamically over an ice sheet geometry, depending on the desired modelling accuracy. When both models are coupled together, the time step restriction is bound to that of the SIA model (quadratic scaling in terms of Δx), whereas the W-SIAStokes model allows for linear scaling.

ACKNOWLEDGMENTS

VON NEUMANN STABILITY ANALYSIS

Without FSSA

Coupling

The solution to the strong form shallow-ice approximation (SIA)

$$-\frac{\partial p}{\partial x} + \frac{\partial}{\partial y}\left(\mu\frac{\partial u_x}{\partial y}\right) = 0 \tag{41}$$

$$-\frac{\partial p}{\partial y} = \rho g \tag{42}$$

is in the isothermal case

$$p = \rho g(h - y)$$

$$u_1 = -\frac{1}{2}\mathfrak{A}(\rho g)^3\left(\frac{\partial h}{\partial x}\right)^3\left((h-b)^4 - (h-y)^4\right),$$

$$u_2 = \int_b^y \frac{\partial u_x}{\partial x}dy = \frac{1}{2}\mathfrak{A}(\rho g)^3\left(3\left(\frac{\partial h}{\partial x}\right)^2\frac{\partial^2 h}{\partial x^2}\left((h-b)^4(y-b) + \frac{(h-y)^5}{5} - \frac{(h-b)^5}{5}\right)\right.$$

$$\left. + 4\left(\frac{\partial h}{\partial x}\right)^3\left((h-b)^3\left(\frac{\partial h}{\partial x} - \frac{\partial b}{\partial x}\right)(y-b) + \frac{(h-y)^4}{4}\frac{\partial h}{\partial x} - \frac{(h-b)^4}{4}\frac{\partial h}{\partial x}\right)\right)$$

defining $H = (h - b)$ and cosindering only the surface $y = h$ we get:

$$u_1 = -\frac{1}{2}\mathfrak{A}(\rho g)^3\left(\frac{\partial h}{\partial x}\right)^3 H^4$$

$$u_2 = \frac{1}{2}\mathfrak{A}(\rho g)^3\left(3\left(\frac{\partial h}{\partial x}\right)^2\frac{\partial^2 h}{\partial x^2}\left(H^5 - \frac{H^5}{5}\right) + 4\left(\frac{\partial h}{\partial x}\right)^3\left(H^4\frac{\partial H}{\partial x} - \frac{H^4}{4}\frac{\partial h}{\partial x}\right)\right)$$

Inserting the closed-form expressions for into the time discretization of the free-surface equation (34) reveals the full coupled system

$$\frac{h^{k+1} - h^k}{\Delta t} + \left(-\frac{1}{2}A(\rho g)^3\left(\frac{\partial h}{\partial x}\right)^3(h-b)^4\right)\frac{\partial h^{k+\gamma}}{\partial x} \tag{43}$$

$$= \frac{1}{2}\mathfrak{A}(\rho g)^3\left(3\left(\frac{\partial h}{\partial x}\right)^2\frac{\partial^2 h}{\partial x^2}\left(H^5 - \frac{H^5}{5}\right) + 4\left(\frac{\partial h}{\partial x}\right)^3\left(H^4\frac{\partial H}{\partial x} - \frac{H^4}{4}\frac{\partial h}{\partial x}\right)\right) + a_s \tag{44}$$

This is a highly non-linear equation and needs to be linearized before Fourier analysis can be used.

Wihtout FSSA all h and H-terms which do not have a superscript $(\cdot)^{k+\gamma}$ are approximated explicitely, i.e. they all will have a superscipt $(\cdot)^k$.

Linearization

Following (Cheng and others, 2017) (where the ice thickness equation was analyzed) we consider a slab on a slope with a small surface perturbation δ around an average state $\bar{h}$ which is just an inclined plane. We write:

$$h = \bar{h} + \delta \text{ (for } h \text{ related to velocity)}, \quad H = \bar{H} + \delta \tag{45}$$

$$h = \bar{h} + \hat{\delta} \text{ (for } h \text{ explicitly in the free surface equation)}, \quad H = \bar{h} + \hat{\delta}. \tag{46}$$

Inserting in (44) yields

$$
\frac{\partial(\bar{h} + \hat{\delta})}{\partial t} + \left(-\frac{1}{2} A(\rho g)^3 \left(\frac{\partial(\bar{h} + \delta)}{\partial x} \right)^3 ((\bar{H} + \delta))^4 \right) \frac{\partial(\bar{h} + \hat{\delta})}{\partial x}
$$
$$
= \frac{1}{2} \mathfrak{A}(\rho g)^3 \left(3 \left(\frac{\partial \bar{h} + \delta}{\partial x} \right)^2 \frac{\partial^2 \bar{h} + \delta}{\partial x^2} \left((\bar{H} + \delta)^5 - \frac{(\bar{H} + \delta)^5}{5} \right) \right.
$$
$$
\left. + 4 \left(\frac{\partial \bar{h} + \delta}{\partial x} \right)^3 \left((\bar{H} + \delta)^4 \frac{\partial(\bar{H} + \delta)}{\partial x} - \frac{(\bar{H} + \delta)^4}{4} \frac{\partial \bar{h} + \delta}{\partial x} \right) \right) + a_s
$$

Using that the second derivative of the steady state surface $\bar{h}$ is zero we get

$$
\frac{\partial(\hat{\delta})}{\partial t} + \left(-\frac{1}{2} A(\rho g)^3 \left(\frac{\partial \bar{h}}{\partial x} \right)^3 (\bar{H})^4 \right) \frac{\partial \hat{\delta}}{\partial x} + \left(-\frac{1}{2} A(\rho g)^3 \left(\frac{\partial(\bar{h} + \delta)}{\partial x} \right)^3 (\bar{H})^4 \right) \frac{\partial \bar{h}}{\partial x}
$$
$$
+ \left(-\frac{1}{2} A(\rho g)^3 \left(\frac{\partial \bar{h}}{\partial x} \right)^3 ((\bar{H} + \delta))^4 \right) \frac{\partial \bar{h}}{\partial x}
$$
$$
= \frac{1}{2} \mathfrak{A}(\rho g)^3 \left(3 \left(\frac{\partial \bar{h}}{\partial x} \right)^2 \frac{\partial^2 \delta}{\partial x^2} \frac{4}{5} \bar{H}^5 + 4 \left(\frac{\partial \bar{h} + \delta}{\partial x} \right)^3 \left((\bar{H})^4 \frac{\partial(\bar{H})}{\partial x} - \frac{(\bar{H})^4}{4} \frac{\partial \bar{h}}{\partial x} \right) \right.
$$
$$
\left. + 4 \left(\frac{\partial \bar{h}}{\partial x} \right)^3 \left((\bar{H} + \delta)^4 \frac{\partial(\bar{H})}{\partial x} + (\bar{H})^4 \frac{\partial(\bar{H} + \delta)}{\partial x} - \frac{(\bar{H} + \delta)^4}{4} \frac{\partial \bar{h}}{\partial x} - \frac{(\bar{H})^4}{4} \frac{\partial \bar{h} + \delta}{\partial x} \right) \right) + a_s
$$

Ignoring higher order terms in δ furthermore yields

$$\frac{\partial(\hat{\delta})}{\partial t} + \left(-\frac{1}{2}A(\rho g)^3\left(\frac{\partial \bar{h}}{\partial x}\right)^3(\bar{H})^4\right)\frac{\partial \hat{\delta}}{\partial x} + \left(-\frac{1}{2}A(\rho g)^3 3\left(\frac{\partial(\bar{h})}{\partial x}\right)^2\left(\frac{\partial(\delta)}{\partial x}\right)(\bar{H})^4\right)\frac{\partial \bar{h}}{\partial x} + \left(-\frac{1}{2}A(\rho g)^3\left(\frac{\partial \bar{h}}{\partial x}\right)^3 4\bar{H}^3\delta\right)\frac{\partial \bar{h}}{\partial x}$$

$$= \frac{1}{2}\mathfrak{A}(\rho g)^3\left(3\left(\frac{\partial \bar{h}}{\partial x}\right)^2\frac{\partial^2\delta}{\partial x^2}\frac{4}{5}\bar{H}^5 + 12\left(\frac{\partial \bar{h}}{\partial x}\right)^2\frac{\partial \delta}{\partial x}\left((\bar{H})^4\frac{\partial(\bar{H})}{\partial x} - \frac{(\bar{H})^4}{4}\frac{\partial \bar{h}}{\partial x}\right)\right.$$

$$\left. + 4\left(\frac{\partial \bar{h}}{\partial x}\right)^3\left(4\bar{H}^3\delta\frac{\partial(\bar{H})}{\partial x} + (\bar{H})^4\frac{\partial(\delta)}{\partial x} - \bar{H}^3\delta\frac{\partial \bar{h}}{\partial x} - \frac{(\bar{H})^4}{4}\frac{\partial \delta}{\partial x}\right)\right) + a_s$$

Considering that the steady state thickness is zero further simplifies the expression into

$$\frac{\partial \hat{\delta}}{\partial t} + \left(-\frac{1}{2}A(\rho g)^3\left(\frac{\partial \bar{h}}{\partial x}\right)^3\bar{H}^4\right)\frac{\partial \hat{\delta}}{\partial x} + \left(-\frac{1}{2}A(\rho g)^3 3\left(\frac{\partial \bar{h}}{\partial x}\right)^2\left(\frac{\partial(\delta)}{\partial x}\right)\bar{H}^4\right)\frac{\partial \bar{h}}{\partial x} + \left(-\frac{1}{2}A(\rho g)^3\left(\frac{\partial \bar{h}}{\partial x}\right)^3 4\bar{H}^3\delta\right)\frac{\partial \bar{h}}{\partial x}$$

$$= \frac{1}{2}\mathfrak{A}(\rho g)^3\left(3\left(\frac{\partial \bar{h}}{\partial x}\right)^2\frac{\partial^2\delta}{\partial x^2}\frac{4}{5}\bar{H}^5 - 3\left(\frac{\partial \bar{h}}{\partial x}\right)^2\frac{\partial \delta}{\partial x}\bar{H}^4\frac{\partial \bar{h}}{\partial x} + 4\left(\frac{\partial \bar{h}}{\partial x}\right)^3\left(\frac{3}{4}\bar{H}^4\frac{\partial \delta}{\partial x} - \bar{H}^3\delta\frac{\partial \bar{h}}{\partial x}\right)\right) + a_s$$

rearranging and defining $\frac{\partial \bar{h}}{\partial x} = C_\alpha$ we get:

$$\frac{\partial \hat{\delta}}{\partial t} - \frac{1}{2}\mathfrak{A}(\rho g)^3 C_\alpha^3\bar{H}^4\frac{\partial \hat{\delta}}{\partial x} - \frac{3}{2}\mathfrak{A}(\rho g)^3 C_\alpha^3\bar{H}^4\frac{\partial \delta}{\partial x} = \frac{6}{5}\mathfrak{A}(\rho g)^3 C_\alpha^2\bar{H}^5\frac{\partial^2\delta}{\partial x^2} + a_s$$

which we will write on the form

$$\frac{\partial \hat{\delta}}{\partial t} - C_1\frac{\partial \hat{\delta}}{\partial x} - C_2\frac{\partial \delta}{\partial x} = C_3\frac{\partial^2\delta}{\partial x^2} + a_s$$

with $C_1 = \frac{1}{2}\mathfrak{A}(\rho g)^3 C_\alpha^3\bar{H}^4$, $C_2 = \frac{3}{2}\mathfrak{A}(\rho g)^3 C_\alpha^3\bar{H}^4$ and $C_3 = \frac{6}{5}\mathfrak{A}(\rho g)^3 C_\alpha^2\bar{H}^5$. OBS! C_1 and C_2 are negative!

We can discretize $\hat{\delta}$ using k or $k+1$ (the latter is better of course), while δ must be taken from time-step k as it originates from the velocity.

Fourier analysis

We will now consider the SIA solution in Fourier space. We will thus apply a Fourier transform, and consider one frequency at a time

$$\delta_j^k \to \tilde{\delta}^k e^{inx_j} = \tilde{\delta} e^{inj\Delta x}$$

$$\delta_{j+1}^k \to \tilde{\delta}^k e^{inx_{j+1}} = \tilde{\delta}^k e^{inj\Delta x} e^{in\Delta x}$$

The factor $e^{inj\Delta x}$ will appear in every term of every equation, and we will hence divide by that and not write it out from here on. We will also consider the finite difference discretization which best corresponds to a P1 FEM discretization, meaning that second derivatives will be represented as central differences so that $\frac{\partial \delta}{\partial x}$ and $\frac{\partial^2 \delta}{\partial x^2}$ are discretized and transformed as:

$$\frac{\partial \delta}{\partial x} \approx \frac{\delta_{j+1} - \delta_{j-1}}{2\Delta x} \to \tilde{\delta} \frac{e^{in\Delta x} - e^{-in\Delta x}}{2\Delta x} = \tilde{\delta} \frac{2i sin(n\Delta x)}{2\Delta x}$$

$$\frac{\partial^2 \delta}{\partial x^2} \approx \frac{\delta_{j+1} - 2\delta_j + \delta_{j-1}}{(\Delta x)^2} \to \tilde{\delta} \frac{e^{in\Delta x} - 2 + e^{-in\Delta x}}{(\Delta x)^2} = -\tilde{\delta} \frac{4 sin^2(n\Delta x/2)}{(\Delta x)^2}$$

Inserting this into the linearized equation , assuming implicit handling of the free surface equation $\alpha = 1$ itself and explicit handling of velocities, and setting $a_s = 0$ gives

$$\frac{\tilde{\delta}^{k+1} - \tilde{\delta}^k}{\Delta t} - C_1 \tilde{\delta}^{k+1} \frac{2i sin(n\Delta x)}{2\Delta x} - C_2 \tilde{\delta}^k \frac{2i sin(n\Delta x)}{2\Delta x} = -C_3 \tilde{\delta}^k \frac{4 sin^2(n\Delta x/2)}{(\Delta x)^2}.$$

Using Euler's formulas and rearranging gives:

$$\tilde{\delta}^{k+1} \left(1 - \Delta t C_1 \frac{2i sin(n\Delta x)}{2\Delta x} \right) = \tilde{\delta}^k \left(1 - \Delta t C_3 \frac{4 sin^2(n\Delta x/2)}{(\Delta x)^2} + \Delta t C_2 \frac{2i sin(n\Delta x)}{2\Delta x} \right).$$

In order for each Fourier mode to stay bounded as the simulation runs, i.e. that $|\tilde{\delta}^{k+1}| \leq |\tilde{\delta}^k|$, we require that

$$\frac{\left| 1 - \Delta t C_3 \frac{4 sin^2(n\Delta x/2)}{(\Delta x)^2} + \Delta t C_2 \frac{2i sin(n\Delta x)}{2\Delta x} \right|}{\left| 1 - \Delta t C_1 \frac{2i sin(n\Delta x)}{2\Delta x} \right|} \leq 1. \tag{47}$$

The denominator value of the parenthesis of the left-hand side is always larger than one (which is due to that $\alpha = 1$). We thus only need to bound the nominator. The complex part of the nominator is bounded as long as

$$\frac{|C_2|\Delta t}{2\Delta t} \leq 1,$$

while the real part needs to fulfil

$$\left|1 - \Delta t C_3 \frac{4\sin^2(n\Delta x/2)}{(\Delta x)^2}\right| < 1 \Rightarrow \frac{C_3 \Delta t}{(\Delta x)^2} < 0.5.$$

So depending on the balance between C_2 and C_3 we get a linear or parabolic time-step constraint. C_3 is big for thick ice with flat slopes, i.e. for the dynamics typical of the interior of an ice sheet, we get a parabolic constraint.

With FSSA

Coupling

As observed from (32), the addition of the FSSA terms makes the discretization of the pressure implicit:

$$p(x, y, t) \approx \rho g(h^{k+1} - y). \tag{48}$$

The pressure yields u_1 and u_1 gives u_2, so this implicit discretization will propagate to the velocity solution in the following way

$$u_1 = -\frac{1}{2}\mathfrak{A}(\rho g)^3 \left(\frac{\partial h^{k+1}}{\partial x}\right)^3 \left((h^k - b)^4 - (h^k - y)^4\right),$$

$$u_2 = \int_b^y \frac{\partial u_x}{\partial x} dy = 3\left(\frac{\partial h^{k+1}}{\partial x}\right)^2 \frac{\partial^2 h^{k+1}}{\partial x^2}\left((h^k - b)^4(y - b) + \frac{(h^k - y)^5}{5} - \frac{(h^k - b)^5}{5}\right)$$

$$+ 4\left(\frac{\partial h^{k+1}}{\partial x}\right)^3 \left((h^k - b)^3\left(\frac{\partial h^k}{\partial x} - \frac{\partial b}{\partial x}\right)(y - b) + \frac{(h^k - y)^4}{4}\frac{\partial h^k}{\partial x} - \frac{(h^k - b)^4}{4}\frac{\partial h^k}{\partial x}\right)$$

Then the final expressions at $y = h$ are :

$$u_1 = -\frac{1}{2}\mathfrak{A}(\rho g)^3 \left(\frac{\partial h^{k+1}}{\partial x}\right)^3 (H^k)^4$$

$$u_2 = \frac{1}{2}\mathfrak{A}(\rho g)^3 \left(3\left(\frac{\partial h^{k+1}}{\partial x}\right)^2 \frac{\partial^2 h^{k+1}}{\partial x^2}\left((H^k)^5 - \frac{(H^k)^5}{5}\right) + 4\left(\frac{\partial h^{k+1}}{\partial x}\right)^3 \left((H^k)^4\frac{\partial H^k}{\partial x} - \frac{(H^k)^4}{4}\frac{\partial h^k}{\partial x}\right)\right)$$

and the fully coupled system is then

$$\frac{h^{k+1} - h^k}{\Delta t} + \left(-\frac{1}{2}A(\rho g)^3 \left(\frac{\partial h^{k+1}}{\partial x}\right)^3 (H^k)^4\right)\frac{\partial h^{k+\gamma}}{\partial x} \tag{49}$$

$$= \frac{1}{2}\mathfrak{A}(\rho g)^3 \left(3\left(\frac{\partial h^{k+1}}{\partial x}\right)^2 \frac{\partial^2 h^{k+1}}{\partial x^2}\left((H^k)^5 - \frac{H^5}{5}\right) + 4\left(\frac{\partial h^{k+1}}{\partial x}\right)^3 \left((H^k)^4\frac{\partial H^k}{\partial x} - \frac{(H^k)^4}{4}\frac{\partial h^k}{\partial x}\right)\right) + a_s \tag{50}$$

Linearization

With the same approach as before we get

$$\frac{\partial \hat{\delta}}{\partial t} + \left(-\frac{1}{2}A(\rho g)^3 \left(\frac{\partial \bar{h}}{\partial x}\right)^3 \bar{H}^4\right)\frac{\partial \hat{\delta}}{\partial x}$$

$$+ \left(-\frac{1}{2}A(\rho g)^3 3\left(\frac{\partial \bar{h}}{\partial x}\right)^2 \left(\frac{\partial \delta^{k+1}}{\partial x}\right)\bar{H}^4\right)\frac{\partial \bar{h}}{\partial x}$$

$$+ \left(-\frac{1}{2}A(\rho g)^3 \left(\frac{\partial \bar{h}}{\partial x}\right)^3 4\bar{H}^3\delta^k\right)\frac{\partial \bar{h}}{\partial x}$$

$$= \frac{1}{2}\mathfrak{A}(\rho g)^3 \left(3\left(\frac{\partial \bar{h}}{\partial x}\right)^2 \frac{\partial^2 \delta^{k+1}}{\partial x^2}\frac{4}{5}\bar{H}^5 - 3\left(\frac{\partial \bar{h}}{\partial x}\right)^2 \frac{\partial \delta^{k+1}}{\partial x}\bar{H}^4\frac{\partial \bar{h}}{\partial x} + 4\left(\frac{\partial \bar{h}}{\partial x}\right)^3 \left(\frac{3}{4}\bar{H}^4\frac{\partial \delta^k}{\partial x} - \bar{H}^3\delta^k\frac{\partial \bar{h}}{\partial x}\right)\right) + a_s$$

rearranging and setting $\frac{\partial \bar{h}}{\partial x} = \frac{\partial \bar{h}}{\partial x} = C_\alpha$ yields

$$\frac{\partial \hat{\delta}}{\partial t} - \frac{1}{2}\mathfrak{A}(\rho g)^3 C_\alpha^3 \bar{H}^4\frac{\partial \hat{\delta}}{\partial x} - \frac{3}{2}\mathfrak{A}(\rho g)^3 C_\alpha^3 \bar{H}^4\frac{\partial \delta^k}{\partial x} = \frac{6}{5}\mathfrak{A}(\rho g)^3 C_\alpha^2 \bar{H}^5\frac{\partial^2 \delta^{k+1}}{\partial x^2} + a_s$$

which we will write on the form

$$\frac{\partial \hat{\delta}}{\partial t} - C_1\frac{\partial \delta^{\hat{k}+1}}{\partial x} - C_2\frac{\partial \delta}{\partial x} = C_3\frac{\partial^2 \delta^{k+1}}{\partial x^2} + a_s$$

So the difference in the linearized equation is that the second derivative is treated implicitly.

Fourier analysis

We get the same expression as without FSSA, only that the second derivative is now treated implicitly

$$\frac{\tilde{\delta}^{k+1} - \tilde{\delta}^k}{\Delta t} - C_1 \tilde{\delta}^{k+1} \frac{2isin(n\Delta x)}{2\Delta x} - C_2 \tilde{\delta}^k \frac{2isin(n\Delta x)}{2\Delta x} = -C_3 \tilde{\delta}^k \frac{4\sin^2(n\Delta x/2)}{(\Delta x)^2}.$$

Rearranging gives

$$\tilde{\delta}^{k+1} \left(1 - \Delta t C_1 \frac{2isin(n\Delta x)}{2\Delta x} + \Delta t C_3 \frac{4\sin^2(n\Delta x/2)}{(\Delta x)^2}\right) = \tilde{\delta}^k \left(1 + \Delta t C_2 \frac{2isin(n\Delta x)}{2\Delta x}\right)$$

The absolute value of the parenthesis to the left is negative, and the one on the right-hand side has an absolute value smaller than one if $\frac{\Delta t}{\Delta x}C_2 \leq 1 \Rightarrow \Delta t \leq \frac{\Delta x}{\frac{3}{2}\mathfrak{A}(\rho g)^3 C_\alpha^3 \bar{H}^4}$, i.e. we get a linear time-step constraint.

REFERENCES

Ahlkrona J, Lötstedt P, Kirchner N and Zwinger T (2016) Dynamically coupling the non-linear Stokes equations with the shallow ice approximation in glaciology: Description and first applications of the ISCAL method. *Journal of Computational Physics*, **308**, 1–19 (doi: 10.1016/j.jcp.2015.12.025)

Alnæs M and 9 others (2015) The FEniCS Project version 1.5. *Archive of Numerical Software*, **3**(100) (doi: 10.11588/ans.2015.100.20553)

Alnæs MS, Logg A, Ølgaard KB, Rognes ME and Wells GN (2014) Unified Form Language: A domain-specific language for weak formulations of partial differential equations. *ACM Transactions on Mathematical Software*, **40**(2), 9:1–9:37 (doi: 10.1145/2566630)

Babuška I (1973) The finite element method with Lagrangian multipliers. *Numer. Math.*, **20**(3), 179–192 (doi: 10.1007/BF01436561)

Brezzi F (1974) On the existence, uniqueness and approximation of saddle-point problems arising from Lagrangian multipliers. *ESAIM: Mathematical Modelling and Numerical Analysis (ESAIM: M2AN)*, **8**(R2), 129–151 (doi: 10.1051/M2AN/197408R201291)

Bueler E (2016) Stable finite volume element schemes for the shallow-ice approximation. *Journal of Glaciology*, **62**(232), 230242 (doi: 10.1017/jog.2015.3)

Bueler E (2023) Performance analysis of high-resolution ice-sheet simulations. *Journal of Glaciology*, **69**(276), 930935 (doi: 10.1017/jog.2022.113)

Bueler E, Lingle CS, Kallen-Brown JA, Covey DN and Bowman LN (2005) Exact solutions and verification of numerical models for isothermal ice sheets. *Journal of Glaciology*, **51**(173), 291306 (doi: 10.3189/172756505781829449)

Cheng G, Lötstedt P and von Sydow L (2017) Accurate and stable time stepping in ice sheet modeling. *Journal of Computational Physics*, **329**, 29 – 47 (doi: 10.1016/j.jcp.2016.10.060)

Gagliardini O, Zwinger T and et al FGC (2013) Capabilities and performance of Elmer/Ice, a new generation ice-sheet model. *Geoscientific Model Development*, **6**, 1299–1318 (doi: 10.5194/gmd-6-1299-2013)

Goelzer H and 41 others (2020) The future sea-level contribution of the Greenland ice sheet: a multi-model ensemble study of ISMIP6. *The Cryosphere*, **14**(9), 3071–3096 (doi: 10.5194/tc-14-3071-2020)

Greve R and Blatter H (2009) *Dynamics of Ice Sheets and Glaciers*. Advances in Geophysical and Environmental Mechanics and Mathematics (AGEM^2), Springer, Berlin (doi: 10.1007/978-3-642-03415-2)

Hindmarsh RCA (2001) *Notes on Basic Glaciological Computational Methods and Algorithms*, 222–249. Springer Berlin Heidelberg, Berlin, Heidelberg (doi: 10.1007/978-3-662-04439-1_13)

Hindmarsh RCA and Payne AJ (1996) Time-step limits for stable solutions of the ice-sheet equation. *Annals of Glaciology*, **23**, 7485 (doi: 10.3189/S0260305500013288)

Hirn A (2013) Finite element approximation of singular power-law systems. *Mathematics of Computation*, **82**(283), 1247–1268 (doi: 10.1090/S0025-5718-2013-02668-3)

Hutter K (1983) Theoretical glaciology: Material science of ice and the mechanics of glaciers and ice sheets (doi: 10.2307/1550909)

Kaus BJ, Mühlhaus H and May DA (2010) A stabilization algorithm for geodynamic numerical simulations with a free surface. *Physics of the Earth and Planetary Interiors*, **181**(1), 12 – 20 (doi: 10.1016/j.pepi.2010.04.007)

Larour E, Seroussi H, Morlighem M and Rignot E (2012) Continental scale, high order, high spatial resolution, ice sheet modeling using the Ice Sheet System Model (ISSM). *Journal of Geophysical Research*, **117**, F01022 (doi: doi:10.1029/2011JF002140)

Löfgren A, Ahlkrona J and Helanow C (2022) Increasing stable time-step sizes of the free-surface problem arising in ice-sheet simulations. *Journal of Computational Physics: X*, **16**, 100114 (doi: 10.1016/j.jcpx.2022.100114)

Löfgren A, Zwinger T, Råback P, Helanow C and Ahlkrona J (2023) Increasing numerical stability of mountain valley glacier simulations: implementation and testing of free-surface stabilization in elmer/ice. *EGUsphere*, **2023**, 1–22 (doi: 10.5194/egusphere-2023-1507)

Morlighem M and 31 others (2017) BedMachine v3: Complete bed topography and ocean bathymetry mapping of greenland from multibeam echo sounding combined with mass conservation. *Geophysical Research Letters*, **44**(21), 11,051–11,061 (doi: 10.1002/2017GL074954)

Pollard D and DeConto RM (2009) Modelling West Antarctic ice sheet growth and collapse through the past five million years. *Nature*, **458**(7236), 329–332 (doi: 10.1038/nature07809)

Robinson A, Goldberg D and Lipscomb WH (2022) A comparison of the stability and performance of depth-integrated ice-dynamics solvers. *The Cryosphere*, **16**(2), 689–709 (doi: 10.5194/tc-16-689-2022)

Seroussi H and 38 others (2019) initMIP-Antarctica: an ice sheet model initialization experiment of ISMIP6. *The Cryosphere*, **13**(5), 1441–1471 (doi: 10.5194/tc-13-1441-2019)

Seroussi H and 46 others (2020) ISMIP6 Antarctica: a multi-model ensemble of the Antarctic ice sheet evolution over the 21st century. *The Cryosphere*, **14**(9), 3033–3070 (doi: 10.5194/tc-14-3033-2020)

Weber ME, Golledge NR, Fogwill CJ, Turney CSM and Thomas ZA (2021) Decadal-scale onset and termination of Antarctic ice-mass loss during the last deglaciation. *Nature Communications*, **12**(1), 6683 (doi: 10.1038/s41467-021-27053-6)

Werder MA, Hewitt IJ, Schoof CG and Flowers GE (2013) Modeling channelized and distributed subglacial drainage in two dimensions. *Journal of Geophysical Research: Earth Surface*, **118**(4), 2140–2158 (doi: 10.1002/jgrf.20146)

Wirbel A and Jarosch AH (2020) Inequality-constrained free-surface evolution in a full Stokes ice flow model (*evolve_glacier v1.1*). *Geoscientific Model Development*, **13**(12), 6425–6445 (doi: 10.5194/gmd-13-6425-2020)